LLNL-JRNL-854115

Achievement of the Planetary Defense Investigations of the Double Asteroid Redirection Test (DART) Mission

N. L. Chabot, A. S. Rivkin, A. F. Cheng, N. X. Roth, R. T. Daly, M. W. Busch, E. Dotto, M. Kueppers, P. Michel, C. D. Waller, R. Makadia, A. Meyer, J. M. Sunshine, S. Eggl, H. Agrusa, D. C. Richardson, P. Pravec, C. A. Thomas, P. Sanchez, P. Scheirich, A. Migliorini, R. Luther, K. Wunnemann, I. Herreros, J. Ormo, M. Husarik, G. S. Collins, T. M. Davison, M. M. Knight, S. Ieva, S. D. Raducan, M. Pajola, A. Lucchetti, M. E. DeCoster, L. M. Parro, T. L. Farnham, S. Chocron, J. Beccarelli, M. Hirabayashi, M. Lazzarin, E. Mazzotta-Epifani, P. Palumbo, F. Tusberti, J. L. Rizos, F. Ferrari, A. Rossi, K. M. Kumamoto, M. B. Syal, T. Santana-Ros, C. Giordano, G. Merisio, B. Murphy, N. Murdoch, P. Panicucci, M. P. Lucas, E. V. Ryan, W. H. Ryan, D. L. Bekker, F. Moreno, et al.

September 11, 2023

Planetary Science Journal

LAWRENCE
LIVERMORE
NATIONAL
LABORATORY

Disclaimer

This document was prepared as an account of work sponsored by an agency of the United States government. Neither the United States government nor Lawrence Livermore National Security, LLC, nor any of their employees makes any warranty, expressed or implied, or assumes any legal liability or responsibility for the accuracy, completeness, or usefulness of any information, apparatus, product, or process disclosed, or represents that its use would not infringe privately owned rights. Reference herein to any specific commercial product, process, or service by trade name, trademark, manufacturer, or otherwise does not necessarily constitute or imply its endorsement, recommendation, or favoring by the United States government or Lawrence Livermore National Security, LLC. The views and opinions of authors expressed herein do not necessarily state or reflect those of the United States government or Lawrence Livermore National Security, LLC, and shall not be used for advertising or product endorsement purposes.

LLNL-JRNL-854115

Achievement of the Planetary Defense Investigations of the Double Asteroid Redirection Test (DART) Mission

N.L. Chabot, A.S. Rivkin, A.F. Cheng, O.S. Barnouin, E.G. Fahnestock, D.C. Richardson, A.M. Stickle, C.A. Thomas, C.M. Ernst, R.T. Daly, E. Dotto, A. Zinzi, S.R. Chesley, N.A. Moskovitz, B.W. Barbee, P. Abell, H.F. Agrusa, M.T. Bannister, J. Beccarelli, D.L. Bekker, M. Bruck Syal, B.J. Buratti, M.W. Busch, A. Campo Bagatin, J.P. Chatelain, S. Chocron, G.S. Collins, L. Conversi, T.M. Davison, M.E. DeCoster, J.D.P. Deshapriya, S. Eggl, R.C. Espiritu, T.L. Farnham, M. Ferrais, F. Ferrari, D. Fohring, O. Fuentes-Munoz, I. Gai, C. Giordano, D.A. Glenar, E. Gomez, D.M. Graninger, S.F. Green, S. Greenstreet, P.H. Hasselmann, I. Herreros, M. Hirabayashi, M. Husarik, S. Ieva, S.L. Ivanovski, S.L. Jackson, E. Jehin, M. Jutzi, O. Karatekin, M.M. Knight, L. Kolokolova, K.M. Kumamoto, M. Kueppers, F. La Forgia, M. Lazzarin, J.-Y. Li, T.A. Lister, R. Lolachi, M.P. Lucas, A. Lucchetti, R. Luther, R. Makadia, E. Mazzotta Epifani, J. McMahon, G. Merisio, C.C. Merrill, A.J. Meyer, P. Michel, M. Micheli, A. Migliorini, K. Minker, D. Modenini, F. Moreno, N. Murdoch, B. Murphy, S.P. Naidu, H. Nair, R. Nakano, C. Opitom, J. Ormo, J.M. Owen, M. Pajola, E.E. Palmer, P. Palumbo, P. Panicucci, L.M. Parro, J.M. Pearl, A. Penttila, D. Perna, E. Petrescu, P. Pravec, S.D. Raducan, K.T. Ramesh, R. Ridden-Harper, J.L. Rizos, A. Rossi, N.X. Roth, A. Rozek, B. Rozitis, E.V. Ryan, W.H. Ryan, P. Sanchez, T. Santana-Ros, D.J. Scheeres, P. Scheirich, C.B. Senel, C. Snodgrass, S. Soldini, D. Souami, T.S. Statler, R. Street, T.J. Stubbs, J.M. Sunshine, N.J. Tan, G. Tancredi, C.L. Tinsman, P. Tortora, F. Tusberti, J.D. Walker, D.C. Waller, K. Wuennemann, M. Zannoni, Y. Zhang

February 26, 2024

Achievement of the Planetary Defense Investigations of the Double Asteroid Redirection Test (DART) Mission

Short title: Achievement of DART's Planetary Defense Mission

Submitted to PSJ: September 29, 2023

Revision sent to PSJ November 18, 2023

Author (affiliation)
Nancy L. Chabot (1) Nancy.Chabot@jhuapl.edu
Andrew S. Rivkin (1)
Andrew F. Cheng (1)
Olivier S. Barnouin (1)
Eugene G. Fahnestock (2)
Derek C. Richardson (3)
Angela M. Stickle (1)
Cristina A. Thomas (4)
Carolyn M. Ernst (1)
R. Terik Daly (1)
Elisabetta Dotto (5)
Angelo Zinzi (6) (7)
Steven R. Chesley (2)
Nicholas A. Moskovitz (8)
Brent W. Barbee (9)
Paul Abell (10)
Harrison F. Agrusa (3) (11)
Michele T. Bannister (12)
Joel Beccarelli (13)
Dmitriy L. Bekker (1)
Megan Bruck Syal (14)
Bonnie J. Buratti (2)
Michael W. Busch (15)
Adriano Campo Bagatin (16)
Joseph P. Chatelain (17)
Sidney Chocron (18)
Gareth S. Collins (19)
Luca Conversi (20) (21)
Thomas M. Davison (19)

36	Mallory E. DeCoster (1)
37	J. D. Prasanna Deshapriya (5)
38	Siegfried Eggl (22)
39	Raymond C. Espiritu (1)
40	Tony L. Farnham (3)
41	Marin Ferrais (23)
42	Fabio Ferrari (24)
43	Dora Föhring (21)
44	Oscar Fuentes-Muñoz (25)
45	Igor Gai (26)
46	Carmine Giordano (24)
47	David A. Glenar (9) (27)
48	Edward Gomez (17) (28)
49	Dawn M. Graninger (1)
50	Simon F. Green (29)
51	Sarah Greenstreet (30) (31)
52	Pedro H. Hasselmann (5)
53	Isabel Herreros (32)
54	Masatoshi Hirabayashi (33) (34)
55	Marek Husárik (35)
56	Simone Ieva (5)
57	Stavro L. Ivanovski (36)
58	Samuel L. Jackson (29) (37)
59	Emmanuel Jehin (38)
60	Martin Jutzi (39)
61	Ozgur Karatekin (40)
62	Matthew M. Knight (41)
63	Ludmilla Kolokolova (3)
64	Kathryn M. Kumamoto (14)
65	Michael Küppers (42)
66	Fiorangela La Forgia (43)
67	Monica Lazzarin (43)
68	Jian-Yang Li (44)
69	Tim A. Lister (17)
70	Ramin Lolachi (9) (27)
71	Michael P. Lucas (45)
72	Alice Lucchetti (13)
73	Robert Luther (46)

```
 74    Rahil Makadia (22)
 75    Elena Mazzotta Epifani(5)
 76    Jay McMahon (25)
 77    Gianmario Merisio (24)
 78    Colby C. Merrill (47)
 79    Alex J. Meyer (25)
 80    Patrick Michel (11) (48)
 81    Marco Micheli (21)
 82    Alessandra Migliorini (49)
 83    Kate Minker (11)
 84    Dario Modenini (26)
 85    Fernando Moreno (50)
 86    Naomi Murdoch (51)
 87    Brian Murphy (37)
 88    Shantanu P. Naidu (2)
 89    Hari Nair (1)
 90    Ryota Nakano (33) (34)
 91    Cyrielle Opitom (37)
 92    Jens Ormö (32)
 93    J. Michael Owen (14)
 94    Maurizio Pajola (13)
 95    Eric E. Palmer (44)
 96    Pasquale Palumbo (49)
 97    Paolo Panicucci (24)
 98    Laura M. Parro (52)(53)
 99    Jason M. Pearl (14)
100    Antti Penttilä (54)
101    Davide Perna (5)
102    Elisabeta Petrescu (21) (38) (40)
103    Petr Pravec (55)
104    Sabina D. Raducan (39)
105    K. T. Ramesh (56)
106    Ryan Ridden-Harper (12)
107    Juan L. Rizos (50)
108    Alessandro Rossi (57)
109    Nathan X. Roth (9) (58)
110    Agata Rożek (37)
111    Benjamin Rozitis (29)
```

112 Eileen V. Ryan (59)

113 William H. Ryan (59)

114 Paul Sánchez (60)

115 Toni Santana-Ros (52) (61)

116 Daniel J. Scheeres (25)

117 Peter Scheirich (55)

118 Cem Berk Senel (40)(62)

119 Colin Snodgrass (37)

120 Stefania Soldini (63)

121 Damya Souami (64)

122 Thomas S. Statler (65)

123 Rachel Street (17)

124 Timothy J. Stubbs (9)

125 Jessica M. Sunshine (3)

126 Nicole J. Tan (12),

127 Gonzalo Tancredi (66)

128 Calley L. Tinsman (1)

129 Paolo Tortora (26)

130 Filippo Tusberti (13)

131 James D. Walker (18)

132 Dany C. Waller (1)

133 Kai Wünnemann (46)

134 Marco Zannoni (26)

135 Yun Zhang (67)

136 ***Affiliations***

137 1. Johns Hopkins University Applied Physics Laboratory, Laurel, MD, 20723, USA
138 2. Jet Propulsion Laboratory, California Institute of Technology, Pasadena, CA
139   91109, USA
140 3. Department of Astronomy, University of Maryland, College Park, MD, 20742,
141   USA
142 4. Department of Astronomy and Planetary Science, Northern Arizona University,
143   Flagstaff, AZ, USA
144 5. INAF-Osservatorio Astronomico di Roma, Via Frascati 33, 00078 Monte Porzio
145   Catone, Roma, Italy
146 6. Agenzia Spaziale Italiana, Via del Politecnico, snc, 00133, Rome, Italy
147 7. ASI – Space Science Data Center, Via del Politecnico, snc, 00133, Rome, Italy
148 8. Lowell Observatory, Flagstaff, Arizona 86004, USA
149 9. NASA Goddard Space Flight Center, Greenbelt, MD, 20771, USA
150 10. NASA Johnson Space Center, Houston, TX, 77058, USA
151 11. Université Côte d'Azur, Observatoire de la Côte d'Azur, CNRS, Laboratoire
152   Lagrange, Nice, France
153 12. School of Physical and Chemical Sciences | Te Kura Matū, University of
154   Canterbury, Private Bag 4800, Christchurch 8140, New Zealand.

13. INAF-Astronomical Observatory of Padova, Vicolo Osservatorio 5, 35122 Padova, Italy
14. Lawrence Livermore National Laboratory, Livermore, CA, USA
15. SETI Institute, Mountain View, CA, USA
16. Instituto de Fisica Aplicada a las Ciencias y las Tecnologias (IUFACyT)
17. Las Cumbres Observatory, Goleta, CA, 93117, USA
18. Southwest Research Institute, San Antonio, TX 78238, USA
19. Department of Earth Science and Engineering, Imperial College London, London, SW7 2AZ, UK
20. European Space Agency – ESRIN, Via Galileo Galilei, 00044 Frascati (RM), Italy
21. ESA PDO NEO Coordination Centre, Via Galileo Galilei, 1, 00044 Frascati (RM), Italy
22. Department of Aerospace Engineering, University of Illinois at Urbana-Champaign, Urbana, IL, USA
23. Florida Space Institute, University of Central Florida, 12354 Research Parkway, Orlando, FL, 32826-0650, USA
24. Department of Aerospace Science and Technology, Politecnico di Milano, Italy
25. Smead Department of Aerospace Engineering Sciences, University of Colorado Boulder, Boulder, CO, USA
26. Department of Industrial Engineering, Alma Mater Studiorum - University of Bologna, Forlì, Italy
27. Center for Space Sciences and Technology, University of Maryland, Baltimore County, Baltimore, MD 21250, USA
28. School of Physics and Astronomy, Cardiff University, Queens Buildings, The Parade, Cardiff CF24 3AA, UK
29. The Open University, Milton Keynes MK7 6AA UK
30. Rubin Observatory/NSF's NOIRLab, Tucson, AZ 85719, USA
31. Department of Astronomy and the DIRAC Institute, University of Washington, Seattle, WA 98195, USA
32. Centro de Astrobiologia (CAB), CSIC-INTA, Carretera de Ajalvir km 4, 28850 Torrejon de Ardoz, Spain
33. Daniel Guggenheim School of Aerospace Engineering, Georgia Institute of Technology, Atlanta, GA 30332, USA
34. Auburn University, Aerospace Engineering/Geosciences, Auburn, AL 36849, USA
35. Astronomical Institute of the Slovak Academy of Sciences, SK-05960 Tatranská Lomnica, Slovakia
36. INAF-Osservatorio Astronomico di Trieste, Trieste, Italy
37. University of Edinburgh, Institute for Astronomy, Royal Observatory, Edinburgh, EH9 3HJ, UK
38. Space sciences, Technologies & Astrophysics Research (STAR) Institute, University of Liège, 4000 Liège, Belgium
39. Space Research and Planetary Sciences, Physikalisches Institut, University of Bern, Switzerland
40. Royal Observatory of Belgium, Brussels, Belgium
41. Physics Department, United States Naval Academy, Annapolis, MD, USA
42. European Space Agency (ESA), European Space Astronomy Centre (ESAC), Villanueva de la Cañada, Madrid, Spain
43. University of Padova, Department of Physics and Astronomy, Vicolo dell'Osservatorio, 3, 35121 Padova, Italy
44. Planetary Science Institute, Tucson, AZ, USA
45. Department of Civil & Environmental Engineering & Earth Sciences, University of Notre Dame, Indiana, USA
46. Museum für Naturkunde Berlin, Leibniz Institute for Evolution and Biodiversity Science, Berlin, Germany
47. Sibley School of Mechanical and Aerospace Engineering, Cornell University, Ithaca, NY 14853, USA

48. University of Tokyo, Department of Systems Innovation, School of Engineering, Tokyo, Japan
49. INAF-Istituto di Astrofisica e Planetologia Spaziale, Roma, Italy
50. Instituto de Astrofísica de Andalucía, CSIC, 18008 Granada, Spain
51. Institut Supérieur de l'Aéronautique et de l'Espace (ISAE-SUPAERO), Université de Toulouse, Toulouse
52. University Institute of Physics Applied to Sciences and Technologies, Universidad de Alicante, 03690 San Vicente del Raspeig, Alicante, Spain
53. Universidad Complutense de Madrid, 28040 Madrid, Spain
54. Department of Physics, P.O. Box 64, FI-00014 University of Helsinki, Finland
55. Astronomical Institute of the Czech Academy of Sciences, Fričova 1, CZ-25165 Ondřejov, Czech Republic
56. Department of Mechanical Engineering, Johns Hopkins University, Baltimore, MD, USA
57. IFAC-CNR, Sesto Fiorentino, 50019, Italy
58. Department of Physics, The Catholic University of America, Washington, DC 20064, USA
59. Magdalena Ridge Observatory, New Mexico Institute of Mining and Technology, Socorro, NM
60. Colorado Center for Astrodynamics Research, University of Colorado Boulder, Boulder, CO 80303, USA
61. Institut de Ciències del Cosmos (ICCUB), Universitat de Barcelona (IEEC-UB), Carrer de Martí i Franquès, 1, 08028 Barcelona, Spain
62. Archaeology, Environmental Changes & Geo-chemistry (AMGC), Vrije Universiteit Brussel, Brussels, Belgium
63. Department of Mechanical and Aerospace Engineering, University of Liverpool, Brownlow street, Liverpool L69 3GL UK
64. LESIA, Observatoire de Paris - Section Meudon, 92195 Meudon Cedex, France
65. NASA Headquarters, 300 E St., SW, Washington DC, 20546, USA
66. Departamento de Astronomía, Facultad de Ciencias, Udelar, Uruguay
67. Department of Climate and Space Sciences and Engineering, University of Michigan, Ann Arbor, MI 48109, USA

246 **Achievement of the Planetary Defense Investigations of the Double Asteroid**
247 **Redirection Test (DART) Mission**

248

249 **Abstract:**

250   NASA's Double Asteroid Redirection Test (DART) mission was the first to
251 demonstrate asteroid deflection, and the mission's Level 1 requirements guided
252 its planetary defense investigations. Here we summarize DART's achievement of
253 those requirements. On 2022 September 26, the DART spacecraft impacted
254 Dimorphos, the secondary member of the Didymos near-Earth asteroid binary
255 system, demonstrating an autonomously navigated kinetic impact into an asteroid
256 with limited prior knowledge for planetary defense. Months of subsequent Earth-
257 based observations showed that the binary orbital period was changed by −33.24
258 min, with two independent analysis methods each reporting a 1-σ uncertainty of
259 1.4 s. Dynamical models determined that the momentum enhancement factor, β,
260 resulting from DART's kinetic impact test is between 2.4 and 4.9, depending on
261 the mass of Dimorphos, which remains the largest source of uncertainty. Over
262 five dozen telescopes across the globe and in space, along with the Light
263 Italian CubeSat for Imaging of Asteroids (LICIACube), have contributed to DART's
264 investigations. These combined investigations have addressed topics related to
265 the ejecta, dynamics, impact event, and properties of both asteroids in the
266 binary system. One year following DART's successful impact into Dimorphos, the
267 mission has achieved its planetary defense requirements, though work to further
268 understand DART's kinetic impact test and the Didymos system will continue. In
269 particular, ESA's Hera mission is planned to perform extensive measurements in
270 2027 during its rendezvous with the Didymos-Dimorphos system, building on DART
271 to advance our knowledge and continue the ongoing international collaboration
272 for planetary defense.

273

1. Introduction:

The topic of planetary defense encompasses understanding the impact hazards posed by natural objects and the efforts undertaken to mitigate or manage these threats. While planetary defense activities have been undertaken for decades (National Academies Press 2010; 2022), in particular searching for and tracking near-Earth asteroids, the Double Asteroid Redirection Test (DART) was the first spacecraft mission dedicated to demonstrating a potential mitigation approach. DART was designed to demonstrate asteroid deflection through a kinetic impactor technique, which had been previously recommended as the first priority for a space mission in the mitigation area (National Academies Press 2010). Although past missions such as Deep Impact (A'Hearn et al. 2005) and Hayabusa2 (Arakawa et al. 2020) utilized impactors to investigate the properties of small bodies, those earlier missions were not intended to deflect their targets and did not achieve measurable deflections.

In 2015, NASA began supporting the Johns Hopkins Applied Physics Laboratory to lead the DART project. The selected target for the DART mission was always the secondary member of the binary (65803) Didymos system, due to the well-characterized properties of the eclipsing binary system and its favorable Earth-Didymos distance in 2022 (Cheng et al 2015). Didymos was discovered in 1996, and photometric observations led to its identification as an eclipsing binary system (Pravec et al. 2003) and to a precise determination of the orbital period of its secondary member (Pravec et al. 2006; Scheirich & Pravec 2009). Arecibo radar observations of the Didymos system were also obtained in 2003, confirming it to be a binary system and characterizing its shape and properties (Naidu et al. 2020). The radar observations constrained the diameter of Didymos to be roughly 780 m and the secondary member to have a diameter of roughly 150 m. The secondary's diameter of ~150 m made it a suitable candidate for the application of the kinetic impactor planetary defense technique (National Academies Press 2010; 2022). The name Didymos was given in 2004 in recognition of its binary nature as it means "twin" in Greek. In 2020, the secondary member (previously referred to as "Didymos B" or informally as "Didymoon") was named Dimorphos, meaning "two forms" in Greek; the name was chosen to reflect that Dimorphos would be slightly altered by DART's planned kinetic impact and hence would have pre-impact and post-impact forms.

Spectral observations of the Didymos system showed that Didymos is an S-class asteroid (de León et al. 2006), linked to ordinary chondrites (Dunn et al. 2013), the most common type of meteorites found on Earth. While there were no direct spectral measurements of Dimorphos, binary asteroid formation models predicted that it was likely that the secondary would have the same composition as the primary (Walsh & Jacobson 2015). Overall, these combined observations made the Didymos system one of the best-characterized binary asteroid systems, and also one with size and composition characteristics highly relevant for planetary defense.

The Didymos system was shown to be accessible by a range of spacecraft trajectory designs (Atchison et al. 2016). Additionally, the distance between Didymos and Earth would be <0.1 au in September and October of 2022 (Atchison et al. 2016) with the Didymos system reaching a maximum brightness of V magnitude 14.4 (Rivkin et al., 2021). This minimum Earth-Didymos distance does not occur again for another 40 years (Rivkin et al. 2021). Consequently, the DART mission concept always planned to impact Dimorphos during the September–October 2022 timeframe, to allow Earth-based telescopes to play a critical role in assessing the effectiveness of the kinetic impact deflection technique. Table A1 summarizes key parameters for the Didymos system.

In contrast, the specific details of the DART mission and spacecraft design underwent a number of iterations during its concept development phases, from 2015–2019. In its earliest development phase, DART's baseline mission included a chemical propulsion trajectory that utilized a small launch vehicle (Cheng et al. 2016; Atchison et al. 2016). However, by 2017, the mission design had changed to utilize an ion-propulsion system, NASA's Evolutionary Xenon Thruster-Commercial (NEXT-C) system, as its primary propulsion system with a launch as a secondary payload (Cheng et al. 2018). By 2019, when the mission held its Critical Design Review, the DART spacecraft had returned to utilizing a chemical propulsion trajectory with a dedicated launch vehicle, while also carrying and demonstrating the NEXT-C ion propulsion system in flight (Adams et al. 2019). The accommodation of NEXT-C heavily influenced the design and development of the spacecraft, its subsystems, and operations (Adams et al. 2019; Badger et al 2022). In particular, to generate the necessary power for NEXT-C, the DART spacecraft included two large Roll-Out Solar Arrays (ROSA), each 8.5 m in length, becoming the first spacecraft to carry this technology (Shapiro & Rodovskiy 2023).

344

345

Figure 1. *The DART spacecraft in September 2021, during the pre-ship inspection at the Johns Hopkins Applied Physics Laboratory. In this image, the NEXT-C ion propulsion engine is at the top of the spacecraft, one of the rolled-up ROSAs is on the right side, and LICIACube is contained on the gold-colored blanketed spacecraft side. In this position, DRACO is not visible as it is pointing at the floor. The main structure of the spacecraft is roughly a cube with dimensions of about 1.3 m, from which other structures extend to result in measurements of roughly 1.8 m in width, 1.9 m in length, and 2.6 m in height.*

354

The DART spacecraft included a single instrument payload, the Didymos Reconnaissance and Asteroid Camera for Optical navigation (DRACO). DRACO was a narrow-angle telescope with a 208-millimeter aperture, a field of view 0.29 degrees wide, a 2560 by 2160 raw pixel complementary metal-oxide semiconductor (CMOS) detector, and a design derived from the high-resolution imager on the New Horizons mission (Fletcher et al. 2018; 2022). DRACO images (Ernst et al., 2023) were utilized by the on-board autonomous algorithms named Small-body Maneuvering Autonomous Real Time Navigation (SMART Nav; Chen et al. 2018; Ericksen et al. 2023; Jensenius et al. 2023; Sawyer et al. 2023). As part of the guidance, navigation, and control (GNC) system (O'Shaughnessy & Hefter 2023), SMART Nav was designed to autonomously identify and distinguish between

Didymos and Dimorphos and then, working in concert with the other GNC elements (Superfin et al. 2023; Miller et al. 2023) and navigation efforts (Bellerose et al., 2023), direct the spacecraft toward the smaller body, Dimorphos, all within roughly an hour of impact. The SMART Nav operations were required to work in parallel with the spacecraft system while also streaming images to the ground in real-time prior to impact (Smith et al. 2020), where an optimized data processing pipeline allowed the processed images to be shared quickly with the public and the team (Waller et al. 2023; Bekker et al. 2023). These requirements also influenced the design and development of other aspects of DART, including the flight software (Heistand et al. 2019), autonomy system (Tropf et al. 2023), the Single Board Computer Field Programmable Gate Array (Zhan et al.,2021) and its associated image processing pipeline (Bekker et al. 2021).

In 2019, DART was chosen to launch on a SpaceX Falcon 9 from Vandenberg Air Force Base (renamed Vandenberg Space Force Base in 2021). In February 2021, the decision was made to move from the mission's primary launch window, which opened in July 2021, to the secondary window, which opened in late November 2021. The change in launch periods did not affect DART's planned impact date with Dimorphos, and the decision noted two technical challenges with mission critical components in particular: the need to reinforce DRACO to ensure it would withstand the stress of launch, and delays in ROSA development due to supply chain impacts, in part due to the COVID pandemic. The DART spacecraft, shown in Figure 1, launched on 2021 November 24, 06:21 UT, the first day of the launch window (Atchison et al. 2023a). The ROSAs were fully deployed successfully within hours after launch. A brief demonstration of NEXT-C was performed during DART's initial check-out period but there was no further use due to an anomaly observed in the spacecraft's power system electronics (John et al. 2023). The DART spacecraft followed a single-phase ballistic trajectory with a series of trajectory correction maneuvers prior to reaching the Didymos system roughly 10 months after launch (Atchison et al. 2023a). The DART project was funded by NASA from 2015-2023 with a total mission cost of roughly $260 M for spacecraft development and operations and $67 M for launch services.

The DART mission was driven by Level 1 requirements, which were approved by NASA in 2017, and these shaped the planetary defense investigations planned by the team (Rivkin et al. 2021). The DART Level 1 requirements were:

- **DART-1.** DART shall intercept the secondary member of the binary asteroid (65803) Didymos as a kinetic impactor spacecraft during its 2022 September–October close approach to Earth.
- **DART-2.** The DART impact on the secondary member of the Didymos system shall cause at least a 73 s change in the binary orbital period.
- **DART-3.** The DART project shall characterize the binary orbit with sufficient accuracy by obtaining ground-based observations of the Didymos system before and after spacecraft impact to measure the change in the binary orbital period to within 7.3 s (1σ confidence).
- **DART-4A.** The DART project shall use the velocity change imparted to the target to obtain a measure of the momentum transfer enhancement parameter referred to as "Beta" (β) using the best available estimate of the mass of Didymos B.
- **DART-4B.** The DART project shall obtain data, in collaboration with ground-based observations and data from another spacecraft (if available), to constrain the location and surface characteristics of the spacecraft impact site and to allow the estimation of the dynamical changes in the Didymos system resulting from the DART impact and the coupling between the body rotation and the orbit.

The Level 1 requirement DART-4B mentions the possibility of data from another spacecraft, "if available." In 2018, the Light Italian CubeSat for Imaging of Asteroids (LICIACube) was added to the DART mission as a secondary spacecraft. Contributed by the Italian Space Agency (Agenzia Spaziale Italiana, ASI), LICIACube, shown in Figure 2, was a 6U CubeSat developed by Argotec under the scientific coordination of the Italian Istituto Nazionale di Astrofisica (INAF) (Dotto et al. 2021). LICIACube was equipped with two cameras: the LICIACube Explorer Imaging for Asteroid (LEIA), a narrow field panchromatic camera, and the LICIACube Unit Key Explorer (LUKE), a wide field red-green-blue (RGB) camera (Poggiali et al. 2022). LICIACube was released from the DART spacecraft on 11 September 2022, 15 days prior to DART's impact, to capture the aftermath of DART's collision and provide key information to inform the resulting planetary defense investigations.

Following impact, the DART project was funded for one year, to carry out the mission's planetary defense investigations and complete the Level 1 requirements. In the next sections, we summarize the achievement of each of DART's Level 1 requirements through its combined planetary defense

436 investigations. In the final section, we discuss the international collaboration
437 on DART and look forward to ESA's Hera mission.

438

439 **Figure 2.** *LICIACube in August 2021, prior to its integration on the DART*
440 *spacecraft. LICIACube is a 6U CubeSat contributed by the Italian Space Agency,*
441 *with dimensions of 10 cm x 20 cm x 30 cm.*

442

443 **2. DART-1: Impact Dimorphos**

444 DART successfully impacted asteroid Dimorphos on 2022 September 26, becoming
445 the first mission to demonstrate asteroid deflection (Daly, Ernst, Barnouin, et
446 al. 2023a). Shared live via a NASA broadcast, over a million concurrent viewers
447 around the world watched as the DART spacecraft streamed images to Earth up to
448 the final sub-second before its impact with Dimorphos, as shown in Figure 3.

449 Having precise information about the Didymos-Dimorphos system before DART's
450 impact provided key inputs to plan DART's specific impact time. With this
451 motivation, the DART team led a focused effort to obtain lightcurve measurements
452 in 2021 and to combine the results with observations from earlier years to
453 determine the pre-impact properties of the Didymos system (Pravec et al. 2022).
454 These combined observations yielded greatly improved knowledge of the Didymos
455 system (Scheirich & Pravec 2022) and importantly constrained the knowledge of
456 the orbital phase of Dimorphos relative to Didymos at the time of impact to

within 5.4°, 3σ uncertainty (Naidu et al. 2022). DART's impact time was chosen with consideration to having direct Earth communication coverage, to having Dimorphos at maximum elongation from Didymos as viewed by the DART spacecraft, to having the solar phase angle ≤60°, and to impacting as nearly head-on as possible, with the motion of the spacecraft in the opposite direction of the motion of Dimorphos about Didymos (Atchison et al. 2023a). The resulting impact angle between DART and Dimorphos was 166.2°, with DART's approach velocity being 9.7° out of the binary orbital plane (Atchison et al. 2023a). In-flight DRACO calibrations during cruise to the Didymos system (Ernst et al. 2023) included imaging of stars and using Jupiter and transits of its moon Europa as targets to test SMART Nav functionality (Ericksen et al. 2023; Sawyer et al. 2023).

DRACO (Fletcher et al. 2022) first detected the Didymos system 61 days prior to impact. Optical navigation was used heavily during the final month to ensure the spacecraft was positioned to impact Dimorphos and to inform the associated trajectory correction maneuvers (Rush et al. 2023; Bellerose et al. 2023). The final trajectory correction maneuver was executed 24 hours prior to the planned impact and placed DART on a trajectory to impact Didymos (Atchison et al. 2023a). Four hours and 5 minutes prior to impact, SMART Nav took control of the spacecraft navigation (Ericksen et al. 2023; Jensenius et al. 2023; Daly, Ernst, Barnouin, et al. 2023a). The SMART Nav system first detected Dimorphos 73 minutes prior to impact and 50 minutes prior to impact, SMART Nav began maneuvering toward Dimorphos. The DART spacecraft impacted Dimorphos on 2022 September 26, at 23:14:24 UTC, with a speed of 6.1 km/s and a mass of 579 kg (Daly, Ernst, Barnouin, et al., 2023a). Evaluation of DART's impact shows that the spacecraft impacted within 2 m of the center of the illuminated figure (Jensenius et al. 2023) and within 25 m of the center of figure of Dimorphos, with an impact angle of roughly 17° from the surface normal (Daly, Ernst, Barnouin, et al. 2023a). Autonomously targeting a small asteroid with limited prior knowledge at high speed was a key accomplishment for the DART mission and marked the achievement of the DART-1 Level 1 requirement. DART's successful kinetic impactor performance also provided mission design and navigation lessons learned for future planetary defense missions (Atchison et al 2023b).
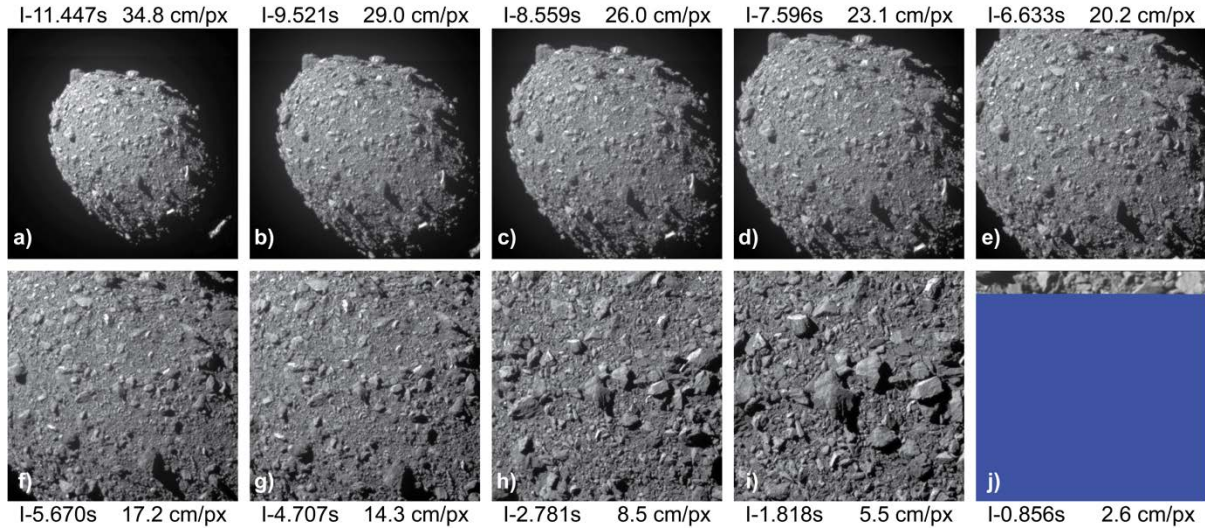
I-11.447s 34.8 cm/px | I-9.521s 29.0 cm/px | I-8.559s 26.0 cm/px | I-7.596s 23.1 cm/px | I-6.633s 20.2 cm/px

I-5.670s 17.2 cm/px | I-4.707s 14.3 cm/px | I-2.781s 8.5 cm/px | I-1.818s 5.5 cm/px | I-0.856s 2.6 cm/px

Figure 3. *Final 10 images returned by DRACO, spanning from 11.5 s prior to impact to a partial image acquired less than a second prior to impact. The timing and pixel scale of each image (a)-(j) is labeled for each panel. In (a), Dimorphos is roughly 177 m in length. In (i), the final complete image has a pixel scale of 5.5 pixel^{-1} and shows an area approximately 28 m in length* **(Ernst et al. 2023).**

3. DART-2: Change the Binary Orbital Period

The DART-2 Level 1 requirement to cause at least a 73 s change in the binary orbital period was derived from requiring that after 1 month, the orbit phase would have been changed by at least one-tenth of an orbit, to ensure that the ground-based telescopes would be able to confidently measure the new period (Rivkin et al. 2021). This requirement factored into the design of the DART spacecraft (Adams et al. 2019) and the mission's trajectory and impact geometry (Atchison et al. 2016; Rivkin et al. 2021). Analysis conducted during DART's 10-month cruise period indicated that given the spacecraft's mass, speed, and planned intercept design, any impact of the DART spacecraft with Dimorphos would result in reducing the orbital period by more than 73 s, including grazing impacts that occurred well off-center from the body.

If DART impacted near the center of Dimorphos and the incident momentum from the DART spacecraft was simply transferred to Dimorphos in a completely inelastic collision with no further momentum enhancement, a binary orbital

period reduction of roughly 7 min was expected (Cheng et al. 2018). However, impact simulations conducted in preparation for DART's kinetic impact test indicated that there could be considerable enhancement to the momentum transferred to Dimorphos due to the ejecta produced, depending on the material strength, impact conditions, and other properties of Dimorphos and DART's impact (Stickle et al. 2022; Raducan & Jutzi 2022). Dynamical models and analysis showed that the resulting binary orbital period could be reduced by more than 40 min for the momentum enhancement factors indicated by some of the impact simulations (Meyer et al. 2021).

Following DART's kinetic impact, both photometric observations and planetary radar observations began, with the goal to determine the post-impact binary orbit period through two independent approaches. Though the ejecta produced by DART's impact event resulted in an immediate brightening of the system that lasted for ~24 days (Graykowski et al. 2023; Kareta et al. 2023), the first photometric observations that could detect a mutual event in the lightcurve were obtained on 2022 September 28, just 29 hours after DART's impact (Thomas et al. 2023a; Moskovitz et al. 2023). The first radar detection of Dimorphos in the echo power spectra occurred even earlier, on September 27, just 12 hours after DART's impact (Thomas et al. 2023a). Radar observations continued through October 13, during the time when the distance between Earth and the Didymos system made such observations possible; echo power spectra were obtained during each radar observing window and range-Doppler images were acquired on 10 different days (Thomas et al. 2023a). The initial set of post-impact photometric observations extended through October 10, until the bright Moon reduced the precision with which photometric observations could be obtained. During the time period from impact through October 10, measurements of 25 mutual events were obtained (Thomas et al. 2023a).

Independent analysis of both the photometric observations and radar observations yielded the same determination of the binary orbital period change. During a NASA press conference on 2022 October 11, just 15 days following DART's impact, the NASA Administrator announced the initial result from the DART team that the binary orbital period of Dimorphos had been reduced by 32 minutes with an uncertainty of ±2 minutes. Continued analysis of these initial data over the next months refined the period change determination to −33.0 ±1.0 (3σ) min (Thomas et al. 2023a). This result definitively verified the DART-2 Level 1

547 requirement, that the DART kinetic impact into Dimorphos had produced at least
548 a 73 s binary orbital period change.

549

550 **4. DART-3: Precisely Measure the Period Change**

551   Photometric observations from 2015–2021 obtained by 11 different telescopes
552 were combined with data from observations obtained in 2003 to determine the
553 pre-impact binary orbital period of Dimorphos about Didymos (Pravec et al.
554 2022). The pre-impact binary orbital period was determined with two separate
555 analysis models, resulting in values of 11.921473 ±0.000138 hr (3σ) (Scheirich
556 & Pravec 2022) and 11.921487 ±0.000028 hr (1σ) (Naidu et al. 2022). Using
557 additional pre-impact observations from 2022 (Moskovitz et al. 2023), the pre-
558 impact binary orbital period was further refined to 11.921493 ±0.000091 hr (3σ)
559 (Scheirich et al. 2023). These pre-impact best-estimates are consistent with
560 each other within their uncertainties, fulfilling a portion of the DART-3 Level
561 1 requirement to determine the binary orbital period precisely before impact.

562   Additionally, this pre-impact knowledge put the post-impact observations in
563 a good position to be able to achieve the remainder of the DART-3 Level 1
564 requirement of determining the change in the binary orbital period to within
565 7.3 s (1σ) without being limited by the pre-impact knowledge of the system. The
566 required value of 7.3 s was derived from ensuring the post-impact orbital period
567 was determined with an accuracy of at least 10%, even if only the minimum 73 s
568 period change resulted from DART's impact (Rivkin et al. 2021).

569   Post-impact photometric observations that were carried out for roughly five
570 months, extending through 2023 February, contributed to the combined dataset
571 used to determine the period change (Moskovitz et al. 2023). From 2022 July
572 through 2023 February, a total of 28 different telescopes distributed across
573 the globe contributed to acquiring >38,000 individual exposures and 224
574 lightcurves, representing over 1000 hours spent targeting the Didymos system
575 (Moskovitz et al. 2023). This unprecedented observational dataset of a binary
576 asteroid system enabled the post-impact period change to be determined with
577 high precision. Applying similar independent analysis models used pre-impact,
578 the final binary orbital period following all these observations was determined
579 to be 11.3675 ±0.0012 hr (3σ) (Scheirich et al. 2023) and 11.3674 ±0.0004 hr
580 (1σ) (Naidu et al. 2023), indicating a period change of −33.24 min or −32.25

min, respectively. The two independent analysis values provide the same result within their uncertainties, with each reporting a 1σ error of 1.4 s, which is well below 7.3 s and thus achieving the DART-3 Level 1 requirement.

The high quality of the post-impact observational dataset additionally allowed an examination of whether the period change remained at a constant value during the timeframe of the observations, from 2022 September through 2023 February. The two analysis models indicate that the binary orbital period immediately after impact was ~20-30 s longer than the final period observed, depending on the approach used to account for the changing period (Naidu et al 2023; Scheirich et al. 2023). The changing period following DART's impact is consistent with the presence of an exponentially decaying drag-like force acting on Dimorphos, with an estimated time constant of ~12 days (Naidu et al., 2023). Analysis of the dynamics of the system supports that the changing period may be caused by interactions with the massive cloud of ejecta, with outward scattering of ejecta decreasing the orbital period (Richardson et al. 2023). By a few months after DART's impact, the data do not indicate any further measurable change in the orbital period (Scheirich et al. 2023, Naidu et al. 2023).

The extensive post-impact observational datasets also contributed key insights into understanding DART's impact event and the dynamics of the binary Didymos system. These aspects are covered under the requirement DART-4B and discussed in Section 6. It is worth noting here though that the rotation of Didymos is a necessary component to account for in the lightcurve analysis to determine the binary orbital period. The analysis shows that the rotation period of Didymos post-impact is indistinguishable from its pre-impact value of 2.260 ±0.001 hr (3σ) (Thomas et al. 2023a), with ongoing work to further reduce that uncertainty.

5. DART-4A: Determine the Momentum Enhancement Factor

The momentum enhancement factor, β, is the ratio of the momentum transferred to the target body relative to the incident momentum of the spacecraft and quantifies how the ejecta produced during a deflection attempt contributes to the momentum imparted to the target (Holsapple & Housen, 2012). In a perfectly inelastic collision, with zero ejecta momentum, β = 1 by definition. However, the ejecta produced during a deflection attempt carries off momentum,

effectively giving an extra push to the target and making β > 1. While β is conceptually simple as just the ratio of the imparted momentum to the incident momentum, the mathematical details become more complicated when the geometry of the Didymos binary asteroid system, DART's impact event, local impact site topography, and resulting ejecta properties are fully considered. Consequently, prior to DART's impact event, Appendix B of Rivkin et al. (2021) provides a detailed three-page mathematical description of the formulation of β and its planned application in the context of the DART mission. The determination of β from DART's results is given in Cheng et al. (2023a), which details the specific mathematical approach ultimately used and shows the details of DART's impact geometry.

The mass, impact velocity, and incoming trajectory of the DART spacecraft are well-determined quantities (Daly, Ernst, Barnouin, et al. 2023a), leaving the major unknown components required to determine β as the change in the orbital velocity of Dimorphos, the mass of Dimorphos, and the net ejecta direction. A Monte Carlo approach was used to produce a distribution of velocity changes that were consistent with the period change determined by the ground-based observations (Thomas et al. 2023a) and that accounted for uncertainties in the Didymos system parameters (Cheng et al. 2023a). The net ejecta direction was constrained using observations from Hubble Space Telescope (Li et al. 2023) and LICIACube images (Dotto et al. 2023), which showed the net ejecta direction to be opposite of DART's incoming trajectory to within roughly 20° (Cheng et al. 2023a; Deshapriya et al. 2023; Hirabayashi et al. 2023). The net ejecta direction and Dimorphos' orbital velocity direction were thus roughly the same, and hence β was calculated in the along-track direction (Cheng et al. 2023a).

The sizes of Didymos and Dimorphos and their separation distance were constrained by DRACO approach images, and DRACO images were also used to determine the shape, and hence volume, of Dimorphos (Daly, Ernst, Barnouin, et al. 2023a; Thomas et al. 2023a). The total mass of the binary system is constrained by the pre-impact orbit period, though given that Didymos is significantly larger than Dimorphos, this does not provide a direct constraint on the mass of Dimorphos. Telescopic observations of the Didymos system taken after DART's impact, during the following days when the signal from the Didymos system was dominated by ejecta from Dimorphos, indicate that Dimorphos, like Didymos, is an S-type asteroid (Lin et al. 2023; Bagnulo et al. 2023; Gray et al. 2023; Lazzarin et al. 2023; Ieva et al. 2023; Polishook et al., 2023). While

651 these telescopic observations provide evidence that the composition of Dimorphos
652 is the same as Didymos, the density of the objects could still be different
653 depending on the macroporosity of the bodies. Thus, the analysis considered a
654 range for the density of Dimorphos from 1500–3300 kg m^{-3}, with a preferred
655 estimate of the density of Dimorphos of 2400 kg m^{-3}, given the knowledge of the
656 Didymos system at the time (Cheng et al. 2023a).

657 From the Monte Carlo approach, an instantaneous reduction in Dimorphos'
658 along-track orbital velocity component of 2.70 ±0.10 mm s^{-1} (1σ) was calculated
659 (Cheng et al. 2023a). Considerations of mass loss, reshaping, and additional
660 observational data suggest minor refinements in the estimate of the along-track
661 velocity change (Meyer et al. 2023b; Naidu et al. 2023; Richardson et al. 2023),
662 but the density of Dimorphos is the largest source of uncertainty currently.
663 Considering the full range of plausible Dimorphos densities, the calculation of
664 β yielded a range of values from 2.4 to 4.9 (Cheng et al. 2023a). If Dimorphos
665 is assumed to have a density of 2400 kg m^{-3}, then the resulting β value is 3.6
666 (Cheng et al. 2023a). The largest uncertainty in the β value resulting from
667 DART's kinetic impact test is due to the uncertainty in the mass of Dimorphos.
668 Thus, minor refinements in the shape of Dimorphos (Daly et al., 2023b) or the
669 period change caused by DART's impact (Naidu et al. 2023; Scheirich et al. 2023)
670 that have occurred since this initial calculation of β (Cheng et al. 2023a) do
671 not have a significant impact on this overall result (Richardson et al. 2023).
672 The determination of the β value produced from DART's kinetic impact test
673 achieved the mission's DART-4A Level 1 requirement.

674 The range of β values determined from the DART mission are within the range
675 of pre-impact predictions from simulations, which spanned β values from 1 to 6
676 (Stickle et al. 2022; Raducan & Jutzi 2022). Experiments have also determined
677 a comparable range of β values, including an experiment with a target that was
678 a collection of stones to mimic a rubble pile and resulted in a β value of 3.4
679 (Walker et al. 2022). Section 6.3 provides a more complete reference listing of
680 pre-impact models and experiments. While there is uncertainty in the β value
681 due to the unknown mass of Dimorphos, the full range of β values determined for
682 the DART experiment are all >2, indicating that more momentum was transferred
683 to Dimorphos from the escaping impact ejecta than was incident with the DART
684 spacecraft. The β value is key to informing the strategy of a kinetic impactor
685 approach to mitigate a future asteroid impact threat to Earth. Should a β value

686 >2 be valid across a wide range of asteroids, it would mean important performance
687 improvements for kinetic impactor asteroid deflection missions.

688

689 **6. DART-4B: Investigate the Didymos-Dimorphos System and the Results of**
690 **DART's Impact**

691   In contrast to the other DART Level 1 requirements, DART-4B was written to
692 be less prescriptive, to encompass the wide range of possible effects resulting
693 from DART's first-of-its-kind kinetic impact test and to enable activities
694 within DART's investigation to understand them. The overall intent of DART-4B
695 captures the requirement to not simply report what DART's kinetic impact test
696 did to Dimorphos but rather to also understand DART's kinetic impact, so it
697 could be applied to other asteroids in the future, if the need arises. In
698 addition to DRACO and LICIACube images, over 5 dozen telescopes on all seven
699 continents and in space participated in the 2022–2023 observation campaign of
700 the DART Investigation Team, as shown in Figure 4. Additionally, telescopic
701 observations were conducted by groups unaffiliated with the DART Investigation
702 Team and are also discussed in the subsections that follow, all working to
703 maximize the data obtained from DART's unique first demonstration of asteroid
704 deflection. Given the wide-ranging results that relate to the DART-4B Level 1
705 requirement, this section is broken into four subsections below.

706

707

Figure 4. *Map depicting the telescopic facilities on Earth and in space that contributed observations to the efforts of the DART Investigation Team. Numerical figures in parentheses next to telescope names indicate the telescope size. Telescopes, alphabetically by state/country, followed by space telescopes – Antarctica: Antarctic Search for Transiting ExoPlanets (ASTEP); Arizona: Lowell Discovery Telescope (LDT), Lowell Observatory 42-inch Hall telescope; Spacewatch, University of Arizona; Vatican Advanced Technology Telescope (VATT); Argentina: Bosque Alegre Astrophysics Station (EABA), Jorge Sahade Telescope at the El Leoncito Astronomical Complex; Australia: Las Cumbres Observatory Global Telescope Network (LCOGT); Bulgaria: Rozhen; California: Table Mountain Observatory (TMO) and the Goldstone Observatory; Palomar Observatory; Canary Islands: Telescopio Nazionale Galileo (TNG), Nordic Optical Telescope (NOT), Las Cumbres Observatory Global Telescope Network (LCOGT), Telescopio Carlos Sánchez (TCS), Jacobus Kapteyn Telescope (JKT), Instituto de Astrofísica de Canarias (IAC), Telescopio Abierto Remoto (TAR); Czechia: Ondrejov; Chile: Atacama Large Millimeter Array (ALMA) Radio Telescope, Very Large Telescope (VLT), Magellan Clay Telescope, Southern Astrophysical Research Telescope (SOAR), La Silla Observatory, Las Cumbres Observatory Global Telescope Network (LCOGT), Swope Telescope; Asteroid Terrestrial-impact Last Alert System (ATLAS), Small and Moderate Aperture Research Telescope System (SMARTS), TRAnsiting Planets and PlanetesImals Small Telecope (TRAPPIST)-South; Georgia:*

22

6.1. Ejecta Observations and Evolution

The ejecta produced by DART's collision was observed by LICIACube, space-based imaging systems, and ground-based telescopic facilities. These observations, ranging from a spacecraft flying by the Didymos system moments after DART's impact to telescopic facilities observing Didymos for nine months post-impact, provide a rich dataset and insight into the ejecta and its evolution.

LICIACube captured images both immediately before and after DART's impact and detected a brightness increase of roughly a factor of five in the LEIA pixel values due to DART's impact (Dotto et al. 2023). LICIACube made its closest approach to Dimorphos 168 s after DART's impact at a distance of approximately 58 km; LICIACube continued to image the Didymos system until 320 s after impact (Dotto & Zinzi 2023). In total, 426 scientific images were returned, and LICIACube continued to communicate with Earth for roughly one month following its Didymos flyby, after which time communication was lost. The LICIACube images reveal a complex and heterogeneous ejecta pattern, as shown in Figure 5. By

764 tracking ejecta features and clumps in the rays through the LICIACube images,
765 early evolution ejecta speeds were found to range from a few tens of m s^{-1} up
766 to roughly 500 m s^{-1} (Dotto et al. 2023). Analysis of the LICIACube images show
767 a wide cone of ejecta, with an opening angle of ~140° (Dotto et al. 2023).
768 Further analysis of LICIACube images have shown that the geometry of the ejecta
769 plume is an elliptical cone that can be described by two angles, a wide opening
770 angle of about 138° and a narrow opening angle of about 102° (Deshapriya et al.
771 2023). Additionally, the intersection of the derived ejecta cone with the
772 surface of Dimorphos corresponds to a region roughly 65 m in radius, which is
773 a substantial portion of the impact hemisphere of Dimorphos (Deshapriya et al.
774 2023). Examination of the RGB images returned by LUKE suggests that the ejecta
775 plume became spectrally redder with increased distance from Dimorphos, which is
776 attributed to either the smaller size of the dust grains in the outer ejecta or
777 to less altered material excavated from Dimorphos' subsurface (Dotto et al.
778 2023). In addition to clumps and diffuse features viewed in the LICIACube
779 images, the images also show numerous individual boulders ejected from
780 Dimorphos. As determined by mapping >90 ~meter-sized boulders, the distribution
781 of the boulders that can be tracked in the LICIACube images show clustering in
782 an ejection direction nearly perpendicular to DART's incoming trajectory, in
783 the direction of Dimorphos' south pole, with a speed of tens of m/s (Farnham et
784 al. 2023). Efforts to provide additional constraints on the ejecta properties
785 from modeling LICIACube images are ongoing (Kolokolova et al. 2022; Lolachi et
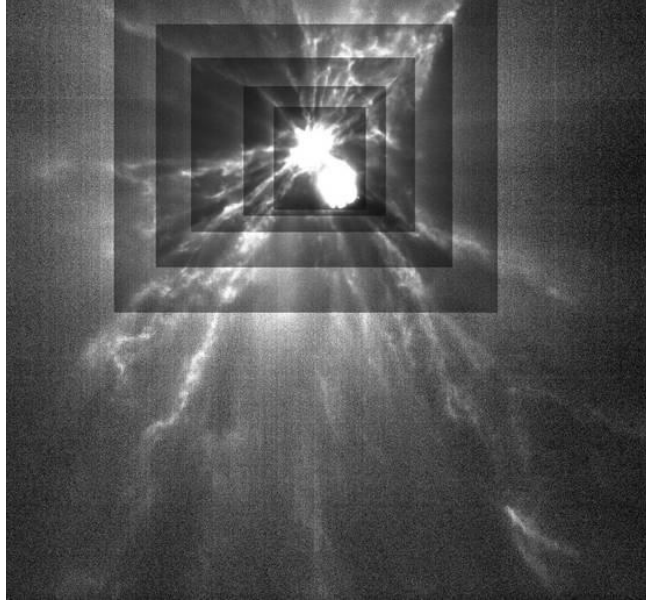786 al. 2023; Ivanovski et al. 2023).

787

788

Figure 5. LICIACube image acquired 143 s following DART's kinetic impact, showing a complex system of ejecta rays. Each rectangle represents a different level of contrast in order to better see the fine structure in the ejecta. The innermost rectangle is roughly 1.3 km wide. (LICIACube LUKE image triplet acquired at 23:16:47 UTC; credit: ASI/NASA/APL)

794

The moment of DART's impact was also captured by a number of Earth-based telescopes (Graykowski et al. 2023; Shestakova et al. 2023; Fitzsimmons et al., 2023) as well as the Lucy mission in space (Weaver et al. 2023). An immediate fast plume of material was observed, as shown in Figure 6a, composed of material with speeds reported as ranging from roughly 1 km/s up to 3.6 km/s (Weaver et al. 2023; Shestakova et al. 2023; Fitzsimmons et al. 2023; Graykowski et al. 2023). In particular, alkali metal neutral emission lines were observed associated with DART's impact event that suggested relative amounts close to solar system abundances, evidence that is consistent with the fast plume being composed of material that originated from Dimorphos (Shestakova et al. 2023). The brightness of the fast plume was seen to correlate with the filter bandpass, such that Earth-based observations taken through filters that encompassed Na or K emissions observed a brighter fast plume (Fitzsimmons et al. 2023). A lower brightness observed by Lucy in comparison to ground-based observations has also been attributed to the wider bandpass of that instrument, though different phase angle viewing conditions may have contributed as well (Weaver et al. 2023).

While the fast ejecta plume contributed substantially to the overall initial brightening of the Didymos system, the upper limit estimates of the mass associated with the fast ejecta plume are just a few hundreds to a few thousands of kg of material (Graykowski et al. 2023; Fitzsimmons et al. 2023; Weaver et al. 2023), a small fraction of the total ejecta mass estimated, as discussed in the next paragraphs.

In the hours that followed DART's impact, both Hubble Space Telescope (HST) (Li et al. 2023) and James Webb Space Telescope (JWST) (Thomas et al. 2023b) (Figure 6b) captured views of the Didymos system and the resulting ejecta. The wide opening angle of the ejecta cone viewed by LICIACube in the minutes following impact was confirmed in these telescopic observations. Analysis that combined the LICIACube and HST observations and accounted for the different viewing conditions of each also showed an elliptical ejecta plume (Hirabayashi et al. 2023), with cone geometry results similar to those obtained by analyzing only LICIACube images (Deshapriya et al. 2023). Ground-based telescopes and HST also obtained views of the evolution of the ejecta over its first few hours, evolving from a cone to the initial indications of a tail of material leaving the Didymos system within a few hours of DART's impact (Li et al. 2023; Opitom et al. 2023; Rozek et al. 2023, Murphy et al. 2023; Lister et al. 2023). The complex evolution of the ejecta is consistent with being influenced by the gravitational interaction between Didymos and Dimorphos as a binary system and with the ejected dust being driven out into a tail by solar radiation pressure (Li et al. 2023). Observations of the ejecta tail continued for many months following DART's impact (Opitom et al. 2023; Lister et al. 2023; Kareta et al. 2023; Rozek et al. 2023; Moreno et al. 2023; Lin et al. 2023; Gray et al. 2023, Murphy et al. 2023) as shown by the examples in Figure 6c-f. The ejecta tail ultimately extended over 70,000 km in length. Deep HST images acquired in December 2022 revealed a population of meter-sized and larger boulders, comoving with the Didymos system with speeds consistent with being among the slowest moving material to escape the system (Jewitt et al. 2023).

As the tail driven by solar radiation pressure continued to lengthen, the Didymos system remained clearly elevated in brightness due to ejecta in the system for ~24 days following DART's impact (Graykowski et al. 2023; Kareta et al. 2023; Lister et al. 2023). At roughly 8 days post-impact, a pause in the dimming of the brightness was noted by multiple telescopes (Kareta et al. 2023; Rozek et al 2023; Lister et al. 2023), which also coincided with the observation

847   of a secondary tail in the ejecta (Li et al. 2023; Murphy et al 2023). It has
848   been suggested that these features at 8 days post-impact may be due to a
849   secondary release of material, such as fallback of larger ejecta from the
850   initial impact event (Kareta et al. 2023; Lin et al. 2023), which models suggest
851   would occur for the first few weeks following DART's impact (Moreno et al. 2023;
852   Ferrari et al. 2023). However, it has also been suggested that the gravitational
853   interactions between slower ejecta and the Didymos binary system naturally can
854   produce a secondary tail without the need for additional impact or disruption
855   events (Ferrari et al. 2023) or that the appearance of a secondary tail may be
856   due to the projection of the ejecta cone and the viewing geometry of the
857   observations (Kim & Jewitt 2023). Spectral and color observations (Lin et al.
858   2023, Polishook et al. 2023, Ieva et al. 2023) as well as polarimetry
859   observations (Bagnulo et al. 2023; Gray et al. 2023;) provide evidence that the
860   ejecta excavated from Dimorphos share similar properties to Didymos as an S-
861   type asteroid. Extended polarimetry observations show that an immediate drop in
862   polarization was associated with DART's impact event and that lower polarization
863   persisted through all the subsequent months of observations; this suggests that
864   smaller or brighter particles than the pre-impact surface were ejected by DART
865   and that these particles continue to exist in the system, either in orbit or
866   deposited on the surface (Gray et al. 2023; Penttilä et al. 2023). Spectral
867   variations observed about 25 days after DART's impact suggest the presence of
868   a cloud of dust around the system, partially and unevenly obscuring the surface,
869   and similar spectral observations in late December 2022 do not show such
870   spectral variations (Lazzarin et al. 2023), consistent with the majority of the
871   ejecta having dissipated within a month following DART's impact event and the
872   system brightness returning to its pre-impact level (Graykowski et al. 2023;
873   Kareta et al. 2023; Lister et al. 2023).

874   Analysis and models of the ejecta observations, informed by pre-impact
875   studies (Fahnestock et al. 2022; Ferrari et al. 2022; Moreno et al. 2022; Rossi
876   et al. 2022; Tancredi et al. 2022), were used to characterize the ejecta dust
877   properties, including the particle size distribution and mass. The particle
878   sizes in the ejecta tail are estimated to range from micrometers to a few
879   centimeters, with radiation pressure sorting the particle size distribution
880   along the tail (Li et al. 2023; Ferrari et al. 2023; Moreno et al. 2023; Lin et
881   al. 2023). Observations of the reflectance slope of the evolving ejecta showed
882   that the initial ejecta was bluer than the pre-impact system, while the tail
883   that formed became redder over the weeks following impact, consistent with being

884 composed of progressively larger particles (Opitom et al. 2023). Observations
885 made with the Atacama Large Millimeter/Submillimeter Array (ALMA) and the
886 Atacama Compact Array (ACA) determined the thermal emission from the Didymos
887 system and the resulting ejecta, providing an estimate for the mass of the
888 ejecta of $1-6x10^7$ kg (Roth et al. 2023). A total ejecta mass estimate of $>10^7$
889 kg is consistent with the mass of ejecta estimated from modeling the fading
890 rate of Didymos over the first few weeks from optical observations (Graykowski
891 et al. 2023) and consistent with the results and lower limits derived from
892 modeling the ejecta evolution (Ferrari et al. 2023; Kim & Jewitt 2023; Moreno
893 et al. 2023), as tabulated in Richardson et al. (2023). Investigating the
894 longer-term evolution of the dust produced by DART's impact event suggests that
895 very small amounts of dust may become meteors on Mars in the next century or
896 the Earth-Moon system over the next millennium (Peña-Asensio et al. 2023).

897 The final observations of the ejecta tail obtained in 2023 were made by HST
898 in July 2023, as shown in Figure 6f, and they show a well-resolved ejecta tail
899 without a clear sign of detachment even nine months following DART's impact
900 event. Observations of the Didymos system will be possible again in 2024, which
901 opens the possibility to continue studying the evolution of the ejecta created
902 by DART's kinetic impact, to understand DART's planetary defense test as well
903 as to gain insight into active asteroids and natural impact events on small
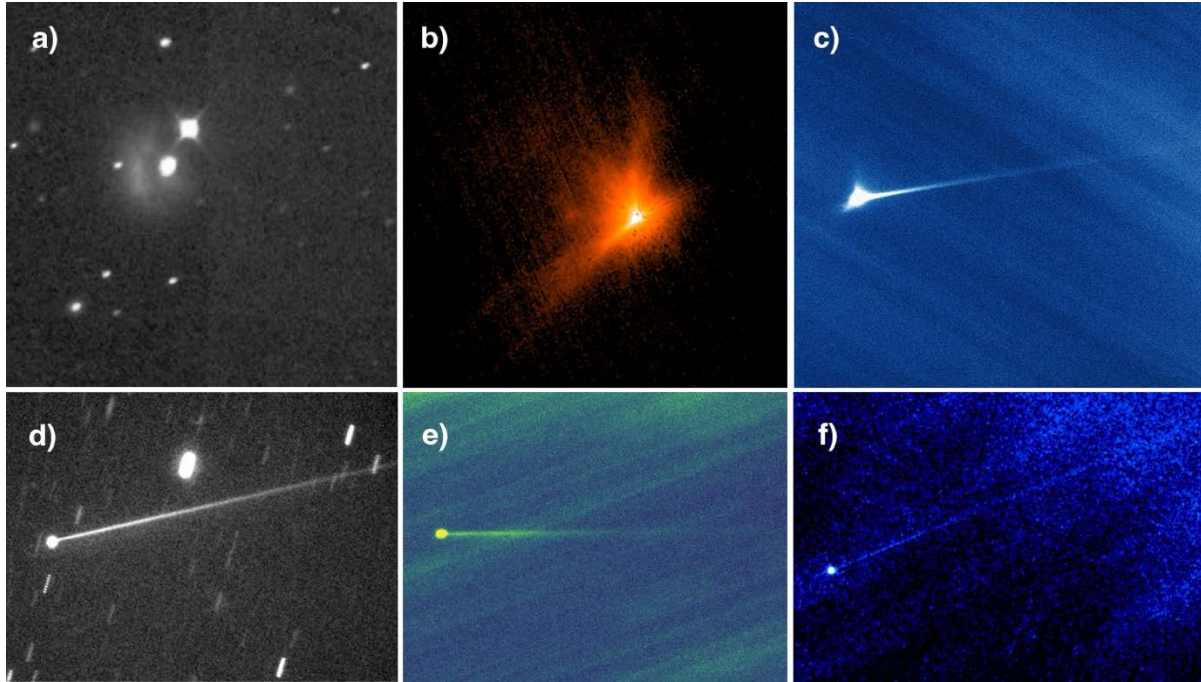904 bodies (Li et al. 2023).

905

Figure 6. *A small sampling of the observations of the ejecta resulting from DART's kinetic impact event. a) Las Cumbres Observatory Global Telescope Network, South Africa – September 26, 2022, 15 min post-impact. The frame is roughly 19,000 km across. b) JWST NIRCam – September 27, 2022, 1.5 hrs post-impact, acquired in the F090W filter (pivot wavelength 0.90 µm). The frame is roughly 300 km across. c) Ōtehīwai Mt. John Observatory, New Zealand – October 6, 2022. The frame is roughly 24,000 km across. d) Magdelena Ridge Observatory, USA – Nov 30, 2022. The frame is roughly 24,000 km across. e) Lowell Discovery Telescope, USA – March 14, 2023. The tail is measured in this deep stack of frames totaling 20,000 s to be roughly 70,000 km in length. f) Hubble Space Telescope – combined products from images acquired June 30-July 6, 2023, with 2.4 hrs total exposure time, with filter F350LP (pivot wavelength 587 nm). The frame is roughly 70,000 km across.*

6.2. Dimorphos and the Impact Site

Reconstruction of the DART spacecraft's trajectory into the local topography of Dimorphos shows that the DART spacecraft bus impacted between two large, roughly 6-m boulders, with the solar arrays impacting these boulders tens of microseconds prior to the main mass of the DART spacecraft (Daly, Ernst,

29

926 Barnouin et al. 2023a). Following the IAU-approved nomenclature theme of
927 percussion musical instruments for features on Didymos and Dimorphos, in January
928 2023, these two boulders were named Atabaque and Bodhran, and are shown on
929 Figure 7. Caccavella is a 2-m boulder also near the impact site. Other named
930 features include Pūniu, which is a small boulder well-resolved in the DRACO
931 images but located further from the impact site that is used to define the
932 Dimorphos coordinate system, and Dhol, the distinctive boulder seen on the limb
933 of Dimorphos.

934 The shape of Dimorphos was derived from stereophotoclinometry using
935 calibrated DRACO images (Ernst et al. 2023), following the methods established
936 pre-impact (Daly et al. 2022). The approach greatly benefitted from the
937 distinctive curvature of the terminator as captured in the images and from
938 reflected light from Didymos faintly illuminating the non-sunlit surface of
939 Dimorphos in the DRACO images (Daly et al. 2023b). The final shape model of
940 Dimorphos (Daly et al 2023b) provides minor improvements over the preliminary
941 version (Daly, Ernst, Barnouin, et al. 2023a), particularly for boulders along
942 the sunlit limb, fine-scale lit terrain along the terminator, and the shape of
943 the dark limb lit by Didymos; however, the volume differs by <3% between the
944 preliminary and final models (Daly et al. 2023b) and hence does not affect the
945 determination of β discussed in Section 5, given the remaining large uncertainty
946 in the mass of Dimorphos. Dimorphos' extents in the X, Y, Z dimensions are 179
947 m, 169 m, and 115 m (Daly et al. 2023b). This result is in contrast to the
948 elongated shape that was assumed for Dimorphos prior to impact based on
949 comparisons to other binary asteroid systems, where the X and Y extents differ
950 more substantially (Rivkin et al. 2021; Richardson et al. 2022). Analysis of
951 LICIACube images of Dimorphos, obtained from a different viewing geometry than
952 DRACO and illuminated by scattered light within the ejecta cloud, are also
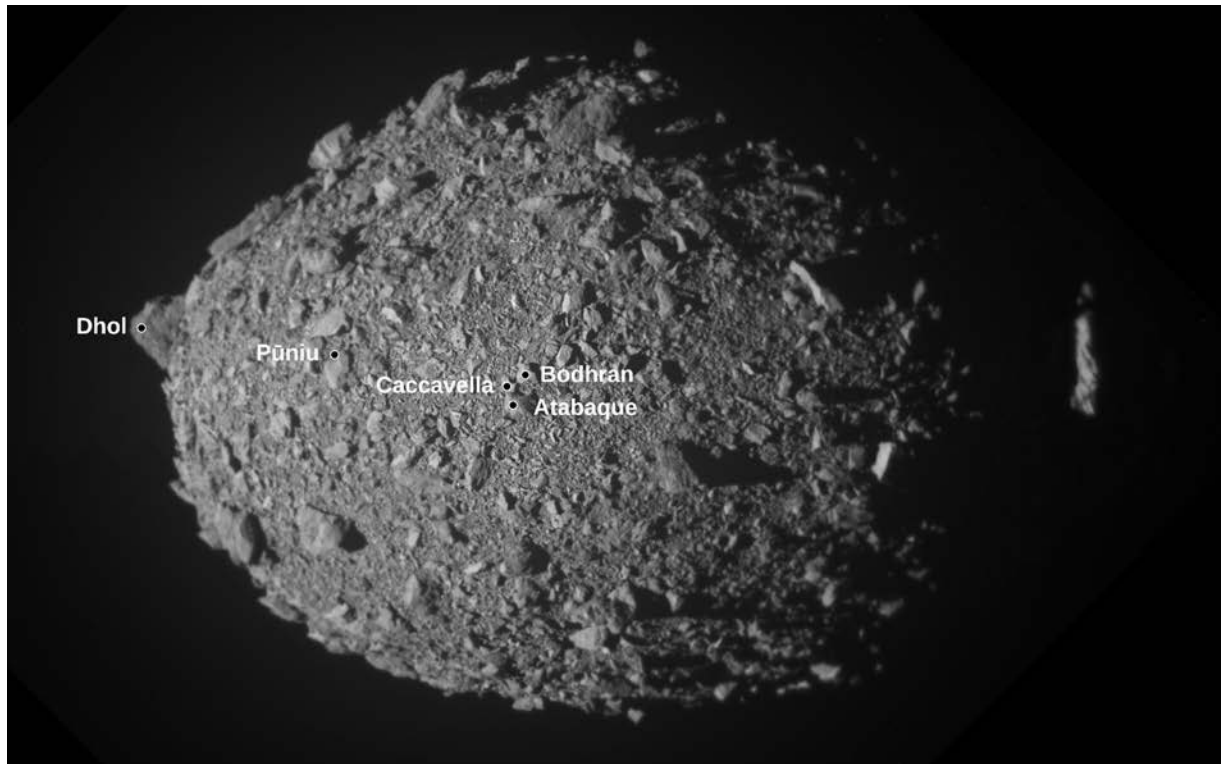953 consistent with this derived final shape model (Zinzi et al. 2023).

954

955
956
957
958
959

960

Calibrated DRACO images (Ernst et al. 2023) that have been projected onto the Dimorphos shape model (Daly et al. 2023b) have enabled detailed geologic investigations of Dimorphos and the DART impact site, in many cases by taking advantage of the analysis capabilities of the Small Body Mapping Tool (Ernst et al. 2018). The size-frequency distribution of boulders on Dimorphos is fit by a Weibull distribution, which suggests that the boulders might have originated from impacts but were also later modified by other processes, such as repeated impacts, thermal fragmentation, or re-accumulation processes (Pajola et al. 2023). Mapping of individual cracks seen on boulders also suggests that thermal-driven stresses are affecting the boulders on Dimorphos (Lucchetti et al. 2023). The boulders on Dimorphos are elongated, with a width-to-length ratio of ~0.6, which is similar to that measured for the small rubble-pile asteroids of

961
962
963
964
965
966
967
968
969
970
971
972

973 Itokawa, Ryugu, and Bennu (Robin et al. 2023). These axial ratios imply that
974 the boulders were formed through impact processing and support the hypothesis
975 that Dimorphos' formation involved a catastrophic disruption event (Robin et
976 al. 2023). Additionally, measurements of the angularity of the boulders provide
977 insight into the bulk internal friction angle of Dimorphos' surface materials,
978 with an estimate of ~35°, which is also similar to that determined for these
979 other small asteroids (Robin et al. 2023).

980 Though the surface of Dimorphos is dominated by boulders, 12 topographic
981 depressions have been identified as plausible impact craters, ranging in size
982 from 3 to 11 m, and a few long lineaments have been mapped on its surface
983 (Barnouin et al. 2023). Applying a photometric correction to the DRACO images
984 to account for the lighting geometry shows evidence for a set of long albedo
985 striations running across Dimorphos, which have been suggested to be due to
986 variations in surface roughness (Buratti et al. 2023). The surface geology of
987 Dimorphos is suggestive of a loosely consolidated rubble pile, though the
988 possibility of some larger, stronger aggregates in its interior cannot be ruled
989 out currently, and the presence of lineaments has implications for the body's
990 strength and subsurface structure (Barnouin et al. 2023). These geologic studies
991 provide insight into understanding Dimorphos as it relates to DART's kinetic
992 impact test but also to understanding the asteroid population in general, as
993 Dimorphos is the smallest asteroid ever investigated by a spacecraft.

994

995 **6.3.   DART's Kinetic Impact Event**

996 All of the previously discussed results, from the details of DART's impact,
997 to the period change, to the determination of β, to observations of the ejecta
998 and the nature of Dimorphos, factor into understanding DART's kinetic impact
999 event. As such, it is a complicated problem with many factors and parameters to
1000 consider. Pre-impact models (Jutzi & Michel 2014; Bruck Syal et al. 2016;
1001 Raducan et al. 2019, 2020, 2021 2022a, 2022b; Raducan & Jutzi 2022; Rainey et
1002 al. 2020; Kumamoto et al. 2022; Stickle et al. 2015, 2017, 2020, 2022; Owen et
1003 al. 2022; Luther et al. 2022; Graninger et al. 2023; DeCoster et al. 2023b) and
1004 experiments (Walker et al. 2013, 2022; Flynn et al. 2015, 2020; Durda et al.
1005 2019; Ormö et al. 2022; Hoerth et al. 2015; Chourey et al. 2020) showed a range
1006 of possible β values and have been crucial for informing the post-impact models
1007 and interpretations. Also, despite the wealth of data associated with DART's

1008 kinetic impact test, there still remain some key unknown quantities, in
1009 particular the mass and material properties of Dimorphos, ranging from the
1010 small-scale properties to the global-scale interior structure. Non-unique
1011 combinations of these asteroidal mechanical properties can produce similar
1012 values of β in impact simulations (Stickle et al. 2022).

1013   Numerical models conducted post-impact were informed by the shape of
1014 Dimorphos and its boulder-strewn surface and the trajectory and impact
1015 conditions of the DART spacecraft and incorporated those details into the
1016 starting conditions (Raducan et al. 2023a; Stickle et al. 2023; DeCoster et al.
1017 2023a). The models show that the generally complex heterogeneous nature of the
1018 ejecta rays viewed by LICIACube, as seen in Figure 5, are consistent with DART's
1019 impact into a non-uniform surface, with the location and size of the boulders
1020 influencing the resulting ejecta pattern (Raducan et al. 2023a; Stickle et al.
1021 2023). This is in line with laboratory observations of ray formation after
1022 impact into heterogeneous materials (Kadono et al. 2019; Ormö et al. 2022).
1023 Impact simulations have been successful at modeling the wide opening angle of
1024 the ejecta cone discussed in Section 6.1 (Raducan et al. 2023a; Stickle et al.
1025 2023), though some models have suggested that for cohesive strengths >500 Pa,
1026 the wide ejecta cone is poorly reproduced (Raducan et al. 2023a). Impact
1027 simulations have also produced results consistent with the β values determined
1028 for DART's impact, as discussed in Section 5, but the models have differed in
1029 the conclusions they have drawn for the implied strength of Dimorphos. Some
1030 models where the near-surface strength can range from near-zero (~10 Pa) to
1031 "moderately weak" (tens of kPa) have been shown to produce β values consistent
1032 with DART's results (Stickle et al. 2023), while other models have concluded
1033 that cohesive strengths < a few Pa are required to provide the best-fit outcome
1034 in terms of β and the excavation timescale (Raducan et al. 2023a).

1035   Analysis using LICIACube images of the plume have also been used to provide
1036 constraints on Dimorphos' material properties, using the approach established
1037 in pre-impact models (Cheng et al 2020; 2022). LICIACube imaging of the ejecta
1038 plume shows no evidence for plume clearing at low altitude, and at roughly 3
1039 minutes after DART's impact, the images show that the ejecta plume remains
1040 optically thick (Cheng et al. 2023b). Modeling efforts concluded that these
1041 LICIACube imaging results, in combination with considering the momentum
1042 enhancement that resulted from DART's impact, are consistent with models where
1043 Dimorphos' strength is <500 Pa and that the best fit results are obtained for

1044   the 5–50 Pa strength cases, which were the lowest considered in the study (Cheng
1045   et al. 2023b).

1046   The cohesive strength also factors into predicting the outcome of DART's
1047   impact on Dimorphos' surface. For a set of simulations that suggest >10 Pa to
1048   tens of kPa, a crater with a diameter of ~30–60 m is predicted (Stickle et al.
1049   2023), which is a sizable crater on Dimorphos, whose volume-equivalent diameter
1050   is only 150 m (Daly et al. 2023b). For models that suggest a strength < a few
1051   Pa, the simulations suggest that DART's impact caused global deformation and
1052   reshaping of Dimorphos rather than a well-defined crater (Raducan et al. 2023a).
1053   Global reshaping from DART's impact event has also been suggested to potentially
1054   result in some deformation in the antipodal hemisphere based on numerical
1055   simulations of a gravitational aggregate target (Liu et al. 2023).

1056   Given the high-quality and extensive post-impact photometric observations
1057   (Moskovitz et al. 2023), the observations have been able to provide constraints
1058   on the post-impact axial dimensions of Dimorphos, through both dynamical
1059   modeling of the orbit (Naidu et al. 2023) and by directly measuring the
1060   rotational lightcurve of Dimorphos in a subset of the observations (Pravec et
1061   al. 2023). The estimated post-impact equatorial axis ratio of Dimorphos from
1062   modeling the orbit is 1.3 (Naidu et al. 2023), differing significantly from the
1063   pre-impact oblate shape with an equatorial axis ratio of 1.02 (Daly et al.
1064   2023b). The Dimorphos rotational lightcurve is also suggestive of Dimorphos
1065   having different post-impact axial ratios (Pravec et al. 2023), outside of the
1066   uncertainties associated with the axial ratios that were determined using the
1067   pre-impact DRACO images (Daly et al. 2023b). That the intersection of the
1068   derived ejecta cone with the surface of Dimorphos corresponds to a region
1069   roughly 65 m in radius also suggests large-scale modification of Dimorphos'
1070   surface (Deshapriya et al. 2023). Different post-impact axial ratios for
1071   Dimorphos are evidence of the creation of a large crater or reshaping of the
1072   body due to DART's impact. Perturbations on the gravitational fields between
1073   the two bodies that could stem from a DART-induced reshaping of Dimorphos are
1074   strong enough to influence the orbit period of Dimorphos and provide a minor
1075   contribution to the resulting period change (Nakano et al. 2022). An estimate
1076   of approximately -100 s of the observed –33.24 m period change may be attributed
1077   to this effect though the precise amount is sensitive to the extent of the
1078   reshaping (Nakano et al. 2023), and this has implications for fully interpreting

the β value due to DART's impact (Nakano et al. 2023; Meyer et al. 2023b; Richardson et al. 2023).

DART's kinetic impact test demonstrated that the ejecta carried considerable momentum, and work is ongoing to more fully understand and evaluate how each ejecta component contributed to the β value determined. Analysis of the ejecta plume geometry suggests that Dimorphos' curvature resulted in an elliptical ejecta cone and a reduction of the momentum transferred relative to an impact on a flat target (Hirabayashi et al. 2023). Thus, a kinetic deflection strategy that gives consideration to the size of the object relative to the cone of the ejecta plume to be produced could result in higher β values by potentially utilizing multiple smaller impactors rather than a single one, and this may become even more relevant for smaller asteroid targets (Hirabayashi et al. 2023). For smaller asteroid targets, understanding when disruption rather than deflection will occur is also important, as modeling suggests that DART's impact event may have been capable of disrupting an approximately 80-m diameter or smaller rubble-pile object (Raducan et al. 2023b). Prior knowledge of the target asteroid can provide valuable information to inform a kinetic impactor strategy (Statler et al. 2022), building on the knowledge gained from DART's first kinetic impact test to inform future planetary defense missions (Rivkin & Cheng 2023; Chabot et al. 2023).

6.4.   The Binary Didymos System

The binary nature of the Didymos system was critical to the design of DART's asteroid deflection mission, enabling Earth-based telescopes to measure and evaluate the deflection efficiency, as discussed in previous sections. In addition, investigations of Didymos and Dimorphos provide new insights into the formation and evolution of binary asteroids, which compose roughly 15% of the near-Earth asteroid population (Pravec et al. 2006). Figure 8 shows the Didymos-Dimorphos binary system to scale as imaged by DRACO. DRACO imaging of Didymos was more limited than for Dimorphos, as Didymos was not visible in the DRACO images sent to Earth as the spacecraft got closer to impacting Dimorphos (Ernst et al. 2023). The last image to contain all of Didymos' sunlit surface was acquired 2.7 min prior to DART's impact, providing a pixel scale of 4.9 m pixel^{-1} on Didymos. The final DRACO image that showed any of Didymos' surface was obtained 1.2 min prior to impact, showing a very small portion of the surface

1114   near Didymos' sunlit limb at 2.2 m pixel^{-1}. Thus, the spatial resolution of
1115   DRACO images for Didymos are much lower than the sub-meter pixel scale images
1116   obtained of Dimorphos, as shown in Figure 3.

1117   One of the immediate results upon seeing the DRACO images was the realization
1118   that the shape of Didymos differed from that developed based on radar
1119   observations (Naidu et al. 2020). The Didymos radar shape model contained the
1120   distinctive bulge of Didymos seen at the equator in Figure 8, resulting in a
1121   "top-shape" as seen on other asteroids such as Ryugu (Watanabe et al. 2019) and
1122   Bennu (Barnouin et al. 2019). However, the X, Y, Z dimensions determined for
1123   Didymos from the radar shape model were 832 m, 838 m, and 786 m (Naidu et al.
1124   2020). In contrast, the Didymos shape model derived by stereophotoclinometry
1125   using DRACO and LICIACube images yields X, Y, Z extents of 819 m, 801 m, and
1126   only 607 m (Barnouin et al. 2023). This substantial difference in the z-axis,
1127   which was the dimension least constrained by the radar measurements, was
1128   apparent even in the approach images of DRACO, as seen in Figure 8. Dynamical
1129   modeling of Dimorphos' orbit yields best-fit parameters for the dimensions of
1130   Didymos that are smaller than either those obtained by using the spacecraft
1131   images or the radar observations, giving X, Y, Z dimensions for Didymos of 788
1132   m, 788 m, and 580 m (Naidu et al 2023).

1133   The smaller size of Didymos derived from spacecraft imaging and dynamical
1134   orbital modeling versus the previous radar observations affects the calculated
1135   density of Didymos, as the mass of the binary system is derived by fitting the
1136   binary orbit. DRACO imaging also provided a new dataset to use to determine the
1137   separation distance of Didymos and Dimorphos prior to DART's impact (Thomas et
1138   al. 2023a; Naidu et al 2023). The best-fit orbit semimajor axis of 1190 ± 30 m
1139   had been previously determined from radar observations (Naidu et al. 2020) and
1140   analysis of DART datasets constrained the value to 1189 ± 17 m (Naidu et al.
1141   2023). Both of these factors contribute to determining the density of the
1142   Didymos system. Prior to DART's impact, the density of the Didymos system was
1143   estimated as 2170 ± 350 kg m^{-3} (Naidu et al. 2020), but using the results derived
1144   from dynamical modeling of Dimorphos' orbit, the current best estimate of the
1145   Didymos system density is considerably higher, now estimated as 2790 ± 140 kg
1146   m^{-3} (Naidu et al. 2023). Thermophysical modeling of the Yarkovsky effect yields
1147   a bulk density of 2750 ± 350 kg m^{-3} for the Didymos system (Rozitis et al. 2023),
1148   also supporting a higher density for Didymos than previous work. The mass of
1149   Didymos comprises >99% of the system's mass, and hence the density of Dimorphos

remains largely unconstrained by these calculations. However, a density of 2790 kg m^{-3} for Didymos has important implications for the stability, formation, and evolution of the Didymos binary system (Richardson et al. 2023). In particular, material cohesive strength is no longer a crucial requirement for maintaining Didymos' structural stability at the spin period of 2.26 h, in contrast to pre-impact models that utilized a lower density for Didymos (Agrusa et al. 2023). Didymos' surface boulders and flattened shape with an equatorial ridge provide evidence that the body is a rubble pile, though the non-circular, angular equatorial perimeter of Didymos also indicates that its interior probably contains some larger distinct aggregates as well (Barnouin et al. 2023).

The geologic features on the surface of Didymos appear more varied than the boulder-strewn surface of Dimorphos and include some of the features a pre-impact synthesis paper proposed might be seen in the images (Pajola et al. 2022). Three geological regions on Didymos have been mapped: one region located at low latitudes that possesses fewer large boulders and has a slightly lower albedo, another region at higher latitudes with multiple large boulders and degraded craters, and a transition region between the two other regions (Barnouin et al. 2023). The Didymos geology correlates with its surface elevation, with the rougher terrain corresponding to highlands and the smoother terrain to lowlands (Barnouin et al. 2023). Multiple plausible craters have been identified in the higher latitude region, with the largest being roughly 270 m in diameter (Barnouin et al. 2023). Crater size-frequency analysis suggests that the surface age of Didymos is ~12.5 Myr and Dimorphos is <0.3 Myr (Barnouin et al. 2023). There is evidence for boulder tracks in the higher latitude region, which provide constraints on the surface cohesion of Didymos (Barnouin et al. 2023) and Didymos' bearing capacity, which corresponds to the maximum pressure that a surface can withstand without experiencing shear failure (Bigot, Lombardo, et al. 2023). In particular, the bearing capacity of Didymos is estimated to be substantially less than comparable materials on the Earth or the Moon, implying that it requires only a low amount of force for surface failure to occur for Didymos' low gravity environment (Bigot, Lombardo, et al. 2023). Examination of the surface roughness properties of both asteroids also suggest that some localized areas on Didymos may have experienced more recent resurfacing events, and that Dimorphos' comparatively rougher surface may be due to being younger than Didymos (Vincent et al. 2023).

1185   The boulder size-frequency distribution for Didymos appears consistent with
1186 a continuation of that measured on Dimorphos, though such effort is limited to
1187 boulders 10-m and larger in size, due to the DRACO pixel scales (Pajola et al.
1188 2023). Comparison to the boulder size-frequency distributions observed on other
1189 asteroids indicates that Didymos and Dimorphos may be the most boulder-dense
1190 asteroids visited by spacecraft to date (Pajola et al. 2023). The boulder size-
1191 frequency distributions are consistent with both bodies having experienced
1192 catastrophic disruption in their past and being rubble piles today, and are
1193 also suggestive that Dimorphos has inherited its material by mass-shedding from
1194 Didymos (Pajola et al., 2023). Investigations regarding the albedo, colors, and
1195 photometric properties of Didymos are ongoing, and can be used to inform pre-
1196 impact observations that suggested a subtle spectral variability in Didymos as
1197 a function of its rotational phase (Ieva et al. 2022), though spectral
1198 observations for a complete rotational period of Didymos in December 2022 did
1199 not find evidence for any significant variations (Lazzarin et al 2023). The
1200 pre-impact thermal inertia value derived for Didymos is consistent with other
1201 S-type near-Earth asteroids (Rozitis et al. 2023). Observations using JWST two
1202 months following DART's impact showed that DART's impact did not change the
1203 thermal inertia of the Didymos system and also provided new insight into the
1204 thermal properties of Didymos' surface, showing spectral properties consistent
1205 with S-complex asteroids and suggesting emission from surface particles smaller
1206 than 25 μm in size (Rivkin et al. 2023). Photometric properties of the Didymos
1207 system, derived by combining DRACO's approach imaging with ground-based
1208 observations over a range of solar phase angles, are also typical for S-type
1209 asteroids (Buratti et al. 2023). A Didymos brightness phase curve, constructed
1210 by combining both LICIACube LUKE and ground-based observations, shows some
1211 differences from a typical S-type asteroid, leading to the suggestion that
1212 Didymos' surface may contain shock-darkened or impact melt minerals (Hasselmann
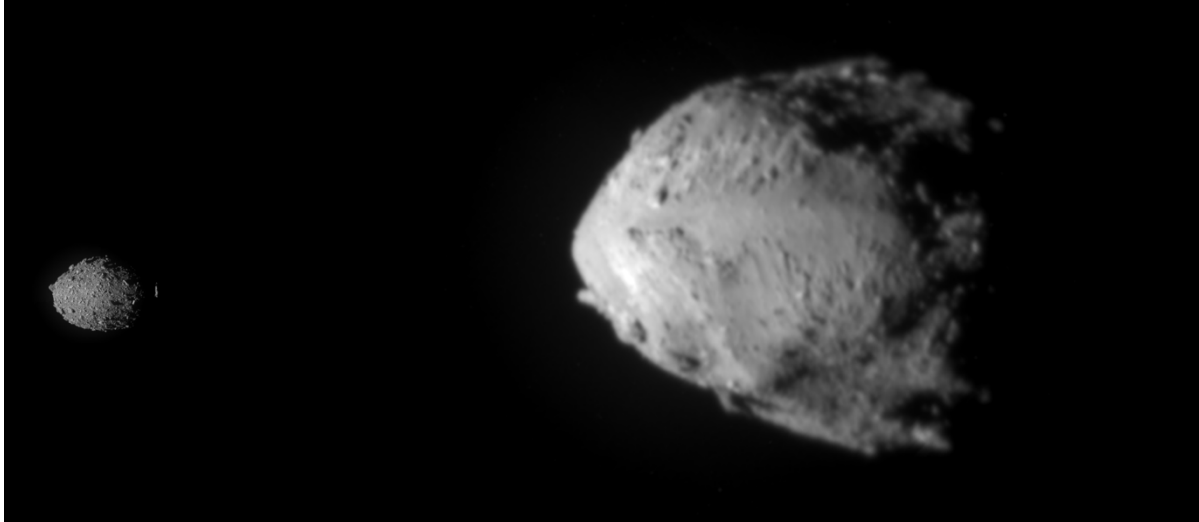1213 et al. 2023).

1214

1215

Figure 8. *A mosaic of DRACO images showing Dimorphos (left, extent in Z direction: 115 m) and Didymos (right, extent in Z direction: 607 m) oriented with their north poles toward the top of the image and with each asteroid and their distance to each other to scale. Dimorphos is a scaled down version of Figure 7. The image of Didymos is a composition of 58 DRACO images assembled by layering the higher-resolution images on top of the lower-resolution ones.*

Pre-impact studies were important in establishing the methodologies to be applied to investigate the post-impact dynamics of the Didymos system and in considering a wide range of possible outcomes (Agrusa et al. 2020; 2021; 2022; Makadia et al. 2022; Meyer et al. 2021; 2023a; Richardson et al. 2022). Overall, the DART kinetic impact test resulted in a small change to the dynamical state of the Didymos system that is generally consistent with pre-impact expectations, with the biggest surprises attributed to the flattened shape of Didymos compared to the radar-based model and the oblate pre-impact shape of Dimorphos (Richardson et al. 2023). Modeling the dynamics of the binary system following DART's impact indicates that the semi-major axis of Dimorphos' orbit was decreased by roughly 37 m (Meyer et al. 2023b) and now has a value of 1152 ±18 m (1σ) (Richardson et al. 2023).

Models of the evolution of the ejecta suggest that roughly 10^6 kg of material are expected to have re-impacted Didymos or Dimorphos within the first 15 days following DART's impact (Moreno et al. 2023; Ferrari et al. 2023), with potential implications for the dynamics of the system (Richardson et al. 2023).

1239 Pre-impact studies suggested that ejecta impacting Didymos could result in
1240 reshaping of the body, which would be accompanied by a change in the rotational
1241 period of Didymos (Hirabayashi et al. 2019; 2022; Nakano et al. 2022); no change
1242 in the rotational period of Didymos has been detected over the months of
1243 telescopic observations that followed DART's impact event (Thomas et al. 2023a;
1244 Naidu et al. 2023; Scheirich et al. 2023), suggesting that measurable reshaping
1245 of Didymos did not occur.

1246   No rotation period of Dimorphos has been obtained from pre-impact
1247 observations. However, post-impact observations that have resolved the
1248 lightcurve of Dimorphos (Pravec et al. 2023) are consistent with Dimorphos being
1249 tidally locked, while also suggesting the possibilities of tumbling of Dimorphos
1250 (Agrusa et al. 2021; Meyer et al. 2023b) and/or reshaping. If DART's impact
1251 produced considerable reshaping of Dimorphos as discussed in Section 6.3, this
1252 reshaping may place the body outside of a currently stable shape and dynamical
1253 configuration, possibly providing a reservoir of material to maintain the tail
1254 (Richardson et al., 2023). Additionally, dynamical models show that reshaping
1255 also increases the chances for Dimorphos to enter a tumbling state (Meyer et
1256 al. 2023b; Nakano et al. 2023), and analyses of the Didymos-system lightcurve
1257 data show some deviations starting roughly 70 days after DART's impact that may
1258 indicate the onset of tumbling (Scheirich et al. 2023). Investigation of the
1259 timescale of how a reshaped Dimorphos would re-equilibrate into a new shape and
1260 dynamical configuration is ongoing.

1261   As it relates to the formation of the Didymos binary system, the oblate shape
1262 of Dimorphos (Daly et al. 2023b) was unexpected and is in contrast to the
1263 prolate shapes associated with other secondary members of binary asteroid
1264 systems (Ostro et al. 2006; Naidu et al. 2015; Becker et al. 2015; Pravec et
1265 al. 2016; 2019). The observation that pre-impact Dimorphos did not have an
1266 irregular shape and had a boulder-covered surface is consistent with modeling
1267 its formation as quickly accreting from material shed by a fast-spinning Didymos
1268 (Madeira et al. 2023), though such a model also produces a prolate rather than
1269 oblate shape for Dimorphos. A suite of *N*-body simulations that followed the
1270 gravitational accumulation of a satellite after a mass-shedding event by a
1271 rapidly rotating primary showed that prolate shapes for the resulting satellite
1272 were preferred but that oblate shapes, like Dimorphos, were also occasionally
1273 formed (Agrusa et al. 2023). The *N*-body simulations showed that the satellite
1274 formed quickly, within a matter of days, and that the accretion process was

highly chaotic, resulting in a wide range of outcomes (Agrusa et al 2023). Whether Dimorphos formed with an oblate shape or evolved into an oblate shape is an ongoing area of study to gain understanding into the formation of binary asteroid systems (Agrusa et al. 2023).

The long-term dynamical evolution of a rubble-pile binary asteroid system is driven by binary Yarkovsky-O'Keefe-Radzievskii-Paddack (BYORP) effect and tides (Richardson et al. 2022). DART data have informed predictions for the effects of DART's impact event on the long-term dynamical evolution of the Didymos-Dimorphos system, though such predictions are sensitive to the exact shape of Dimorphos and the nature of any cratering or reshaping experienced (Cueva et al. 2023). In the case of a binary system, there are two β values to be considered: a β value for Dimorphos, which has been the focus of DART's investigation (Cheng et al. 2023a), and a heliocentric β value for the Didymos system, the momentum enhancement factor caused by the ejecta that escapes the binary system. Pre-impact analysis examined the range of possible heliocentric β values that could result from DART's impact and demonstrated that the Didymos system would not be shifted onto a collision course with the Earth (Makadia et al. 2022), though a measure of the Didymos system's deflection about the Sun potentially could be made in the future (Richardson et al. 2022). A measurement of heliocentric β for the Didymos system has not yet been made, though multiple high-quality stellar occultation observations obtained in 2022-2023, including detections of Dimorphos as the smallest object ever observed during an occultation campaign, may make such a measurement possible in the next few years (Makadia et al. 2023).

During the DART mission, the team used a tabulated summary of the current best knowledge of the Didymos system, referred to as the Design Reference Asteroid (DRA) (Rivkin et al. 2021). The DRA was updated throughout the mission as new information yielded refined results for both pre-impact and post-impact parameters of the Didymos system, and it served to provide common input for the many modeling and analysis efforts being led in parallel across the team, such as the determination of β. Values summarized in the last version of the DRA produced by the DART team are provided in Table A1.

7. International Collaboration and the Hera Mission

International collaboration has been at the core of the DART mission since its origin. In 2003, ESA produced the first study report, led by Andrea Milani (1948–2018), for the Don Quijote mission concept, which would involve two spacecraft, one serving as a kinetic impactor and the other serving as an orbiter to measure the impact outcomes (Milani et al. 2003). ESA continued to study multiple variations on the Don Quijote concept through 2007 (Wolters et al. 2011; Michel et al. 2022). This led to the Asteroid Impact and Deflection Assessment (AIDA) collaboration a few years later (Cheng et al. 2015), with the NASA-led DART kinetic impactor spacecraft (Cheng et al. 2016) and the ESA-led Asteroid Impact Mission (AIM) rendezvous spacecraft (Michel et al. 2016). The AIM spacecraft, which would have rendezvoused with the Didymos system prior to DART's impact and hence characterized the system both before and after DART's kinetic impact test, was not selected for flight in 2016. The Hera mission was subsequently developed as an optimized version of AIM, with reduced risks and cost (Michel et al. 2018), and in 2018, Hera was approved for flight by ESA. Hera is on track to launch in 2024 and rendezvous with the Didymos system in late December 2026, conducting a robust remote sensing campaign in 2027 to investigate the aftermath of DART's kinetic impact event (Michel et al. 2022).

Given the development history of AIDA, DART, LICIACube, and Hera, the DART Investigation Team benefited extensively from continued close international collaboration throughout the mission. The DART Investigation Team included roughly 300 scientists from over 100 different institutions that represented 29 different countries, as listed in Table B1. Thirty-two U.S. members were supported through the DART project as Co-Investigators or in team leadership roles to ensure that the mission achieved its Level 1 requirements. In 2021, NASA selected four additional U.S. scientists to join the DART Investigation Team through a Participating Scientist Program. However, by having the DART Investigation Team open to individuals beyond those directly supported by NASA for the DART mission, both U.S. as well as international scientists were able to join and contribute to the DART Investigation Team through a wide range of funding sources, as detailed in the Acknowledgements section of this paper. This organization of the DART Investigation Team enabled the mission to include international cooperation for the international issue of planetary defense and to maximize what was learned from humanity's first demonstration of asteroid deflection. While NASA's DART project ended in 2023, the DART mission data

1345   archive (Waller et al. 2023) is available within NASA's Planetary Data System,
1346   supporting further investigations and informing future international planetary
1347   defense investigations, such as Hera.

1348   Hera is a highly capable orbiter spacecraft, equipped with a set of optical
1349   cameras, a spectral imager, a LIDAR, a thermal infrared imager, and a radio
1350   science system (Michel et al. 2022). In addition, Hera carries two CubeSats,
1351   which will be deployed in the Didymos system and communicate with the main
1352   spacecraft. The CubeSat Juventas carries a low-frequency monostatic radar as
1353   well as a gravimeter and an accelerometer (Michel et al. 2022). The Milani
1354   CubeSat, named in honor of Andrea Milani for the Don Quijote concept, has a
1355   near-infrared spectral imager and a microthermogravimeter (Michel et al. 2022).
1356   Hera's rendezvous observations will provide key measurements to further
1357   investigate the results of DART's kinetic impact test, in particular by
1358   measuring the mass of Dimorphos, by observing the surface of Dimorphos to reveal
1359   the nature of cratering or reshaping that resulted from DART's impact, by
1360   investigating the interior structure of the asteroids, and by making fundamental
1361   measurements of properties of the post-impact binary system. Additionally,
1362   Hera's extensive remote sensing capabilities are positioned to enable the
1363   mission to go beyond DART-related investigations and to advance our
1364   understanding of the properties of asteroids with implications for the formation
1365   and evolution of our Solar System.

1366   As DART's pioneering planetary defense mission is followed by the Hera
1367   mission, and as more planetary defense missions begin to move from concepts to
1368   reality, it is also important to emphasize that these two missions are just one
1369   part of a much larger planetary defense strategy. The combined efforts of the
1370   DART and Hera missions are providing fundamental insight into understanding the
1371   kinetic impactor technique as a potential method of asteroid deflection, taking
1372   the first steps to develop a capability to potentially prevent an asteroid
1373   impact with the Earth in the future, if such a need should arise. However, for
1374   a kinetic impactor to have any chance at successfully deflecting an asteroid on
1375   a collision course with Earth, warning time is key. To be most effective, the
1376   kinetic impactor should be used many years or decades in advance of the predicted
1377   Earth impact date (National Academies Press 2010; 2022). Thus, finding,
1378   tracking, and characterizing near-Earth objects is vital to the overall
1379   planetary defense strategy, as are international collaboration and coordinated
1380   communication efforts. DART and Hera represent some of the first spacecraft

1381   missions in the ongoing and growing international efforts related to planetary
1382   defense.
1383

1453

1454   **Appendix A**

1455   This appendix provides values summarized in the final Design Reference
1456   Asteroid (DRA) produced by the DART Investigation Team. Values used in an
1457   earlier DRA used by the DART team are provided in Rivkin et al. (2021). The DRA
1458   reflects a summary of the current best knowledge of the Didymos system, covering
1459   values for the system both before and after DART's impact event. The different
1460   values are determined by different studies, and hence the specific values are
1461   not necessarily consistent with each other. In particular, the axial extents
1462   for Didymos determined using spacecraft images (Barnouin et al. 2023) differ
1463   from the ellipsoid axes for Didymos determined by the best-fit dynamical model
1464   for the orbit of Dimorphos (Naidu et al. 2023). For this table, we have decided
1465   to list the values from multiple studies, for easy comparison. This reflects
1466   the current best understanding of the Didymos system, and this summary of key
1467   values tracked in the DRA is provided here as a resource for future
1468   investigations of the Didymos system.

1469

1470   **Table A1.**

1471   Parameters of the Didymos system. All uncertainties are 1σ.

Parameter	Value	Comments and References
System Characteristics		
Mean absolute magnitude, H	18.16 ±0.04	Pravec et al. (2012)
Geometric albedo	0.17 ±0.01	Naidu et al. (2020)
Radar polarization ratio	0.20 ±0.02	Neese et al. (2020)
Spectral type of Didymos	S-class	de León et al. (2006)
Best meteorite analog	L/LL chondrite	Dunn et al. (2013)
S-band radar albedos	0.20 ±0.05	Naidu et al. (2020)
X-band radar albedos	0.30 ±0.08	Naidu et al. (2020)
Heliocentric orbit parameters (pre- and post-impact)	see reference	JPL Solar System Dynamics Horizons System: https://ssd.jpl.nasa.gov/tools/sbdb_lookup.html#/?sstr=didymos
Pre-Impact Parameters		
Semimajor axis of system (m)	1189 ±17	Naidu et al. (2023)
System GM (m^3 s^{-2})	35.4 ±1.5	Naidu et al. (2023)
Didymos spin pole, λ, β (°)	310 ±3, -80.7 ±0.5	Naidu et al. (2023)
Dimorphos orbital eccentricity	<0.03	Assumed based on Scheirich & Pravec (2009)
Bulk density of Didymos (kg m^{-3})	2790 ±140	Naidu et al. (2023)
Bulk density of Dimorphos (kg m^{-3})	2400 ±300	Daly, Ernst, Barnouin, et al. (2023a)
Volume equivalent diameter of Didymos (m)	730 ±8	Barnouin et al. (2023)
Volume equivalent diameter of Dimorphos (m)	150 ±2.5	Daly et al. (2023b)
Didymos extents along x, y, z axes (m)	819 ±14, 801 ±14, 607 ±14	Barnouin et al. (2023)

Didymos ellipsoid a, b, c axes (m)	818 ±14, 796 ±14, 590 ±14	Barnouin et al. (2023)
Didymos ellipsoid a, b, c axes (m)	788 ±22, 788 ±22 580 ±32	Naidu et al. (2023)
Dimorphos extents along x, y, z axes (m)	179 ±1, 169 ±4, 115 ±1	Daly et al. (2023b)
Dimorphos ellipsoid a, b, c axes(m)	173 ±1, 170 ±4, 113 ±1	Daly et al. (2023b)
Dimorphos elongation for ellipsoid, a/b, a/c, b/c	1.02 ±0.02, 1.52 ±0.02, 1.49 ±0.04	Daly et al. (2023b)
Didymos oblateness (J2)	0.090 ±0.008	Naidu et al. (2023)
Dimorphos orbital period (hr)	11.921493 ±0.00003	Scheirich et al. (2023)
Rotation period of Didymos (hr)	2.2600 ±0.0001	Naidu et al. (2020)
Rotation period of Dimorphos	11.921493 ±0.00003	Assumed to have a synchronous orbit
Post-Impact Parameters		
Semimajor axis of system (m)	1152 ±18	Meyer et al. (2023b) gives a change of 37 ±1 m
Dimorphos orbital geometric eccentricity	0.0274 ±0.0015	Naidu et al. (2023)
Dimorphos ellipsoid a, b, c axes(m)	192 ±12, 148 ±8, 118 ±14	Naidu et al. (2023)
Dimorphos elongation for ellipsoid, a/b, a/c, b/c	1.30 ±0.01, 1.6 ±0.3, 1.3 ±0.2	Naidu et al. (2023)
Dimorphos orbital period (hr)	11.3675 ±0.0004	Scheirich et al. (2023)
Dimorphos orbital period (hr)	11.3674 ±0.0004	Naidu et al. (2023)
Rotation period of Didymos (hr)	2.2600 ±0.0003	Thomas et al. (2023a)

1472

1473

Appendix B

This appendix lists the members of the DART Investigation Team in
alphabetical order by their last name.

Table B1

DART Investigation Team Members

Last Name	First Name	Home Institution
Abe	Lyu	Observatoire de la Côte d'Azur
Abell	Paul	NASA Johnson Space Center
Agrusa	Harrison	University of Maryland
Amoroso	Marilena	Italian Space Agency (ASI)
Arakawa	Masahiko	Kobe University
Arredondo	Anicia	SwRI
Asphaug	Erik	University of Arizona
Bagnulo	Stefano	Armagh Observatory and Planetarium
Baki	Paul	Technical University of Kenya
Ballouz	Ron	JHU APL
Bannister	Michele	University of Canterbury, New Zealand
Barbee	Brent	NASA/Goddard Space Flight Center
Barnouin	Olivier	JHUAPL
Barucci	Antonella	LESIA -Paris Observatory
Beccarelli	Joel	INAF of Padova
Bekker	Dmitriy	APL
Bellerose	Julie	Jet Propulsion Laboratory
Belskaya	Irina	V.N. Karazin Kharkiv National University
Benavidez	Paula	Universidad de Alicante
Benner	Lance	Jet Propulsion Laboratory
Berthier	Jerome	IMCCE/Observatoire de Paris
Bertini	Ivano	University of Naples 'Parthenope', Italy
Bhaskaran	Shyam	Jet Propulsion Laboratory
Bigot	Jeanne	ISAE-SUPAERO
Birlan	Mirel	IMCCE, Paris Observatory, France
Bjonnes	Evan	Lawrence Livermore National Laboratory
Bottke	William	Southwest Research Institute
Brucato	John Robert	INAF - Arcetri Astrophysical Observatory
Bruck Syal	Megan	Lawrence Livermore National Laboratory
Brucker	Melissa	University of Arizona
Buratti	Bonnie	JPL
Burger	Christoph	University of Tübingen
Burkeey	Mary	Lawrence Livermore National Laboratory
Busch	Michael	SETI Institute
Caballo Perucha	Piluca	Joanneum Research
Caldwell	Wendy	Los Alamos National Laboratory
Cambioni	Saverio	Massachusetts Institute of Technology
Campo Bagatin	Adriano	Universidad de Alicante
Capannolo	Andrea	Politecnico di Milano
Caporali	Simone	Università degli studi di Firenze
Carroll	Kieran	Gedex Systems Inc.
Carry	Benoit	Observatoire de la Cote d'Azur
Castellini	Francesco	ESOC
Cellino	Alberto	INAF - Osservatorio Astrofisico di Torino
Ceresoli	Michele	Politecnico di Milano

Chabot	Nancy	Johns Hopkins Applied Physics Lab
Charnoz	Sebastien	IPGP/Université Paris Cité
Cheng	Andy	Johns Hopkins Applied Physics Lab
Chesley	Steve	JPL
Chocron	Sidney	Southwest Research Institute
Choi	Young-Jun	Korea Astronomy and Space Science Institute
Ciarletti	Valerie	LATMOS
Cintala	Mark	NASA Johnson Space Center
Cline	Christopher	NASA Johnson Space Center
Colazo	Milagros	IATE (CONICET)
Collins	Gareth	Imperial College London
Contreras	Carlos	Las Campanas Observatory
Cotugno	Biagio	Argotec
Cremonese	Gabriele	INAF-Padova
Cueva	Rachel	University of Colorado Boulder
Cuk	Matija	SETI Institute
Dall'Ora	Massimo	INAF-OACN
Daly	Terik	Johns Hopkins University Applied Physics Laboratory
Daly	Michael	York University
Davis	Alex	University of Colorado
Davison	Thomas	Imperial College London
de Leon	Julia	Instituto de Astrofisica de Canarias
DeCoster	Mallory	Johns Hopkins University Applied Physics Lab
Della Corte	Vincenzo	INAF, Italian National Astrophysics Institute, IAPS
Dello Russo	Neil	JHU/APL
Deshapriya	J. D. Prasanna	INAF-Osservatorio Astronomico di Roma
Dotto	Elisabetta	INAF - Osservatorio Astronomico di Roma
Duffard	René	Instituto de Astrofísica de Andalucía - CSIC
Durda	Dan	Southwest Research Institute
Eggl	Siegfried	University of Illinois at Urbana-Champaign
Erasmus	Nicolas	South African Astronomical Observatory
Ernst	Carolyn	Johns Hopkins University Applied Physics Laboratory
Espiritu	Raymond	JHUAPL
Essert	Jan	ESA
Fahnestock	Gene	JPL / Caltech
Falke	Albert	Airbus Defence and Space GmbH, Germany
Farnham	Tony	University of Maryland
Ferrais	Marin	Arecibo Observatory / University of Central Florida
Ferrari	Fabio	Politecnico di Milano
Filice	Valerio	Royal Observatory of Belgium
Fitzsimmons	Alan	Queen's University Belfast
Föhring	Dora	European Space Agency
Frattin	Elisa	University of Padua
Fu	Xiaoyu	University of Liverpool
Fuentes-Munoz	Oscar	University of Colorado Boulder
Gai	Igor	University of Bologna
Gaitanas	Michalis	Aristotle University of Thessaloniki
Gaskell	Robert	Planetary Science Institute
Gil	Jesus	ESA

Giordano	Carmine	Politecnico di Milano
Gkolias	Ioannis	Aristotle University of Thessaloniki
Glenar	Dave	UMBC
Gomez Casajus	Luis	Università di Bologna, Bologna, Italy
Gramigna	Edoardo	University of Bologna (UNIBO)
Graninger	Dawn	Johns Hopkins University Applied Physics Laboratory
Granvik	Mikael	University of Helsinki / Luleå University of Technology
Gray	Zuri	Armagh Observatory and Planetarium
Green	Simon	The Open University
Grieger	Björn	Aurora Technology B.V. for ESA, ESAC, Spain
Guillot	Tristan	Observatoire de la Côte d'Azur, CNRS, France
Güldemeister	Nicole	Museum für Naturkunde Berlin
Hamilton	Douglas	University of Maryland
Hartzell	Christine	University of Maryland
Hasselmann	Pedro Henrique	INAF-Osservatorio di Roma
Henry	Grégoire	Royal Observatory of Belgium
Herfort	Ulrich	European Space Agency – ESOC
Hergenrother	Carl	Ascending Node Technologies, LLC
Herique	Alain	Universite Grenoble Alpes - IPAG
Herreros	Isabel	Centro de Astrobiologia (CAB), CSIC-INTA
Hestroffer	Daniel	IMCCE/Paris Observatory, Univ. PSL
Hirabayashi	Masatoshi	Auburn University
Holler	Bryan	STScI
Holt	Carrie	University of Maryland
Howell	Ellen	University of Arizona
Howley	Kirsten	LLNL
Hsieh	Syau-Yun	Johns Hopkins Applied Physics Lab
Husárik	Marek	Astronomica Institute of the Slovak Academy of Sciences
Ieva	Simone	INAF - Osservatorio astronomico di Roma
Impresario	Gabriele	Agenzia Spaziale Italiana
Ivanovski	Stavro	National Institute for Astrophysics Italy
Jackson	Samuel	University of Edinburgh
Jacobson	Seth	Michigan State University
Jehin	Emmanuel	University of Liège
JeongAhn	Youngmin	Korea Astronomy and Space Science Institute
Jutzi	Martin	University of Bern
Kadono	Toshihiko	University of Occupational and Environmental Health
Karatekin	Ozgur	Royal Observatory of Belgium
Kareta	Theodore	Lowell Observatory
Karthick	Chrisphin	Indian Institute of Astrophysics (IIA)
Kašpárek	Tomáš	Brno University of Technology
Kikwaya Eluo	Jean-Baptiste	Vatican Observatory
Kim	Myung-Jin	Korea Astronomy and Space Science Institute
Knight	Matthew	United States Naval Academy
Kohout	Tomas	University of Helsinki, Finland
Kokotanekova	Rosita	Bulgarian Academy of Sciences
Kolokolova	Ludmilla	University of Maryland, College Park
Kramer	Emily	Jet Propulsion Laboratory

Krugly	Yurij	Institute of Astronomy of V.N. Karazin Kharkiv National University
Kumamoto	Kathryn	Lawrence Livermore National Laboratory
Küppers	Michael	ESA/ESAC
La Forgia	Fiorangela	University of Padova
Larson	Jennifer	University of Central Florida
Lasagni Manghi	Riccardo	University of Bologna
Lazzarin	Monica	Padova University
Leakey	Acacia	Turkana Basin Institute
Lee	Hee-Jae	Korea Astronomy and Space Science Institute
Li	Jian-Yang	Planetary Science Institute
Libourel	Guy	Université Côte d'Azur, Observatoire de la Côte d'Azur
Lin	Zhong-Yi	Institute of Astronomy, NCU
Lister	Tim	Las Cumbres Observatory
Lolachi	Ramin	UMBC/NASA GSFC/CRESST II
Lombardo	Marco	University of Bologna
Lombardo	Pauline	ISAE-SUPAERO
Long	Chloe	CU Boulder
Lubey	Daniel	JPL
Lucas	Michael	University of Notre Dame
Lucchetti	Alice	INAF - OAPD Astronomical Observatory of Padova
Luther	Robert	Museum für Naturkunde Berlin
Lyzhoft	Josh	NASA Goddard Space Flight Center
Madeira	Gustavo	Institut de Physique du Globe de Paris
Makadia	Rahil	University of Illinois at Urbana-Champaign
Manzoni	Claudia	London Stereoscopic Company
Marchi	Simone	Southwest Research Institute
Marzari	Francesco	Padova University
May	Erin	JHU APL
May	Brian	London Stereoscopic Company
Mazzotta Epifani	Elena	INAF-OAR
McMahon	Jay	University of Colorado
Meneghin	Andrea	INAF
Merisio	Gianmario	Politecnico di Milano
Merrill	Colby	Cornell University
Meyer	Alex	University of Colorado Boulder
Michel	Patrick	Université Côte d'Azur, Observatoire de la Côte d'Azur, CNRS, Lagrange Lab
Migliorini	Alessandra	INAF, Institute for Space Astrophysics and Planetology
Milam	Stefanie	NASA/GSFC
Miller	Paul	Lawrence Livermore National Laboratory
Minker	Kate	Observatoire de la Côte d'Azur
Mitra	Nilanjan	Johns Hopkins University
Modenini	Dario	University of Bologna
Moissl	Richard	ESA/ESTEC
Mondal	Bhaskar	University of Illinois at Urbana-Champaign
Moon	Hong-kyu	Korea Astronomy and Space Science Institute
Moreno	Fernando	Instituto de Astrofísica de Andalucía, CSIC
Mosher	Joel	JPL

Moskovitz	Nicholas	Lowell Observatory
Mueller	Michael	ESOC
Muinonen	Karri	University of Helsinki
Murdoch	Naomi	ISAE-SUPAERO
Murphy	Brian	University of Edinburgh
Naidu	Shantanu	Jet Propulsion Laboratory
Nair	Hari	JHU/APL
Nakamura	Akiko	Kobe University
Nakano	Ryota	Georgia Institute of Technology
Noiset	Guillaume	Royal Observatory of Belgium
Nolan	Michael	University of Arizona
Nugent	Carrie	Olin College
Ogawa	Kazunori	Japan Aerospace Exploration Agency
Oldroyd	Will	Northern Arizona University
Opitom	Cyrielle	University of Edinburgh
Ormö	Jens	Centro de Astrobiología (CAB), CSIC-INTA
Osip	David	Carnegie Observatories: Las Campanas Observatory (LCO)
Oszkiewicz	Dagmara	Adam Mickiewicz University
Owen	John	Lawrence Livermore National Laboratory
Owen	Chu	Travelling Telescope
Paar	Gerhard	JOANNEUM RESEARCH
Pajola	Maurizio	INAF-Astronomical Observatory of Padova
Pajuelo	Myriam	Pontificia Universidad Católica del Perú
Palamakumbure	Lakshika	University of Helsinki
Palmer	Eric	Planetary Science Institute
Palumbo	Pasquale	Parthenope University of Naples; INAF - Instituto di Astrofisica e Planetologia Spaziale (IAPS) in Roma
Panfichi	Aldo	Pontificia Universidad Católica del Peru
Panicucci	Paolo	Politecnico di Milano
Parro	Laura	Complutense University of Madrid / University of Arizona / University of Alicante
Pearl	Jason	Lawrence Livermore National Laboratory
Penttilä	Antti	University of Helsinki
Perna	Davide	INAF - Osservatorio Astronomico di Roma
Petrescu	Elisabeta	European Space Agency, ESOC
Pirrotta	Simone	Italian Space Agency
Pittichova Chesley	Jana	JPL/Caltech
Plesko	Catherine	Los Alamos National Laboratory
Poggiali	Giovanni	INAF - Arcetri Observatory, University of Florence
Polakis	Tom	Lowell Observatory
Polishook	David	Weizmann Institute of Science
Popescu	Marcel	Astronomical Institute of the Romanian Academy
Pou	Laurent	JPL
Pravec	Petr	Astronomical Institute of the Academy of Sciences of the Czech Republic
Pugliatti	Mattia	Politecnico di Milano
Raducan	Sabina	University of Bern
Rainey	Emma	Johns Hopkins University Applied Physics Laboratory
Rambaux	Nicolas	IMCCE - Observatory of Paris
Ramesh	KT	Johns Hopkins University

Raskin	Cody	Lawrence Livermore National Laboratory
Regiec	Alysen	JHUAPL
Richardson	Derek	University of Maryland
Ridden	Ryan	University of Canterbury
Rivkin	Andrew	JHU/APL
Rizos	Juan	Instituto de Astrofísica de Andalucía - CSIC
Robin	Colas	ISAE-SUPAERO
Rosch	Thomas	Johns Hopkins University Applied Physics Laboratory
Rossi	Alessandro	IFAC-CNR
Roth	Nathan	NASA Goddard Space Flight Center
Rożek	Agata	University of Edinburgh
Rozitis	Ben	The Open University
Russell	Shannon	Two Sigma
Ryan	Eileen	New Mexico Institute of Mining and Technology/MRO
Ryan	William	New Mexico Institute of Mining and Technology
Sánchez	Paul	University of Colorado Boulder
Santana-Ros	Toni	Universidad de Alicante / Institut de Ciències del Cosmos (ICCUB), Universitat de Barcelona (IEEC-UB)
Sarid	Gal	SETI Institute
Schaefer	Christoph	University of Tuebingen
Scheeres	Daniel	University of Colorado
Scheirich	Peter	Astronomical Institute ASCR, Ondrejov, Czech Republic
Schultz	Peter	Brown University
Schwartz	Stephen	University of Arizona
Senel	Cem Berk	Royal Observatory of Belgium
Serebryanskiy	Aleksander	Fesenkov Astrophysical Institute
Shestakova	Lyubov	Fesenkov Astrophysical Institute (FAI)
Sickafoose	Amanda	PSI/MIT
Simioni	Emanuele	INAF-OAPD
Simonetti	Simone	Argotec
Smith	Matthew	JPL
Snodgrass	Colin	University of Edinburgh
Soldini	Stefania	University of Liverpool
Souami	Damya	LESIA, Observatoire de Paris
Statler	Thomas	NASA Headquarters
Steckloff	Jordan	Planetary Science Institute
Stickle	Angela	JHU/APL
Stubbs	Timothy	NASA Goddard Space Flight Center
Sunday	Cecily	Institut Supérieur de l'Aéronautique et de l'Espace
Sunshine	Jessica	University of Maryland
Tancredi	Gonzalo	Depto. Astronomia, UdelaR, Uruguay
Tanga	Paolo	Observatoire de la Côte d'Azur
Tardivel	Simon	Centre National d'Etudes Spatiales (CNES)
Tasev	Elisa	Royal Observatory of Belgium
Telus	Myriam	University of California Santa Cruz
Thomas	Cristina	Northern Arizona University
Thomas-Osip	Joanna	Gemini Observatory
Tinsman	Calley	APL
Titus	Timothy	USGS Astrogeology Science Center
Tortora	Paolo	University of Bologna

Trigo-Rodríguez	Josep M.	Institute of Space Sciences (CSIC/IEEC)
Troianskyi	Volodymyr	Astronomical Observatory Institute, A. Mickiewicz University
Tsiganis	Kleomenis	Aristotle University of Thessaloniki
Tubiana	Cecilia	IAPS/INAF, Rome, Italy
Tusberti	Filippo	INAF - Astronomical Observatory of Padova
Veillet	Christian	Large Binocular Telescope Observatory
Venditti	Flaviane	Arecibo Observatory
Veras	Dimitri	University of Warwick
Vincent	Jean-Baptiste	DLR Institute for Planetary Research
Voyatzis	George	Aristotle University of Thessaloniki, Greece
Wada	Koji	Chiba Institute of Technology
Walker	James	Southwest Research Institute
Walker	Harry	European Space Agency
Waller	Dany	Johns Hopkins University Applied Physics Laboratory
Walsh	Kevin	Southwest Research Institute
Washington	Antoine	University of Maryland
Weaver	Hal	JHU Applied Physics Laboratory
Whizin	Akbar	Southwest Research Institute
Wimarsson	John	University of Bern
Wolfmayr	Monika	University of Jyvaskyla, Finland
Wong	Ian	NASA GSFC
Wuennemann	Kai	Museum fuer Naturkunde Berlin
Xiang	Zhen	University of Bern
Yanamandra-Fisher	Padma	Space Science Institute
Yu	Yang	Beihang University
Zannoni	Marco	University of Bologna
Zanotti	Giovanni	Politecnico di Milano
Zhang	Yun	Université Côte d'Azur, Observatoire de la Côte d'Azur, CNRS, Lagrange Lab
Zinzi	Angelo	Agenzia Spaziale Italiana (ASI) - Space Science Data Center
Zou	Xiaoduan	Planetary Science Institute

1480
1481

References:

Adams, E., O'Shaughnessy, D., Reinhart, M. et al. 2019, in IEEE Aerospace
Conference, doi: 10.1109/AERO.2019.8742007

Agrusa, H. F., Richardson, D. C., Davis, A. B., et al. 2020, Icar, 349,
113849

Agrusa, H. F., Gkolias, I., Tsiganis, K., et al. 2021, Icar, 370, 114624

Agrusa, H. F., Ferrari, F., Zhang, Y., Richardson, D. C. & Michel, P. 2022,
PSJ, 3(7), 158

Agrusa, H. F., Zhang, Y., Richardson, D. C., et al. 2023, PSJ, submitted

A'Hearn, M. F., Belton, M. J. S., Delamere, W. A., et al. 2005, Science, 310,
258

Arakawa, M., Saiki, T., Wada, K., et al. 2020, Science, 368, 67

Atchison, J. A., Laipert, F. E., & McQuaide, M. E. 2023a, 45th Rocky Mountain
AAS GN&C Conference, AAS 23-360

Atchison, J., Bellerose, J., Bhaskaran, S., et al. 2023b, AcAau, IAA-PDC-23-
154

Atchison, J. A., Ozimek, M. T., Kantsiper, B. L., & Cheng, A. F. 2016, AcAau,
123, 330-339

Badger A. R., John, J. W., Liang, R., et al. 2022, 2022iep_conf

Bagnulo, S., Gray, Z., Granvik, M., et al. 2023, ApJ Letters, 945(2), L38

Barnouin, O. S., Daly, M. G., Palmer, E. E., et al. 2019, NatGe, 12, 247-252

Barnouin, O., Ballouz, R.-L., Marchi, S., et al. 2023, NatCo, submitted

Becker, T. M., Howell, E. S., Nolan, M. C., et al. 2015, Icar, 248, 499-515.

1520

1521   Bekker, D. L., Daly, R. T., Ernst, C. M., et al. 2023, in LPSC 54, 2511

1522

1523   Bekker, D., Smith, R. & Tran, M. Q. 2021, in 2021 IEEE Space Computing
1524   Conference, 122-133

1525

1526   Bellerose, J., Bhaskaran, S., Rush, B., et al. 2023, AcAau, IAA-PDC-23-146

1527

1528   Bigot, J., Lombardo, P., Murdoch, N., et al. 2023, NatCo, submitted

1529

1530   Bruck Syal, M., Owen, J. M., & Miller, P. L. 2016, Icar, 269, 50-61

1531

1532   Buratti, B., Pittichova, J., Mishra, I., et al. 2023, PSJ, submitted

1533

1534   Chabot, N., Adams, E., Rivkin, A., & Kalirai, J. 2023, IAC, IAC-23-E10.1

1535

1536   Chen, M. H., Atchison, J. A., Carrelli, D. J., et al. 2018, in AIAA Guidance,
1537   Navigation and Control, 164, 18-063

1538

1539   Cheng, A. F., Atchison, J. A., Kantsiper, B. L., et al. 2015, AcAau, 115,
1540   262-269

1541

1542   Cheng, A. F., Michel, P., Jutzi, M., et al. 2016, P&SS, 121, 27-35

1543

1544   Cheng, A. F., Rivkin, A. S., Michel, P., et al. 2018, P&SS, 157, 104-115

1545

1546   Cheng, A. F., Stickle, A. M., Fahnestock, E. G., et al. 2020, Icar, 352,
1547   113989

1548

1549   Cheng, A. F., Raducan, S. D., Fahnestock, E. G., et al. 2022, PSJ, 3(6), 131

1550

1551   Cheng, A. F., Agrusa, H. F., Barbee, B., et al. 2023a, Nature, 616, 457-460

1552

1553   Cheng, A. F., Raducan, S. D., Jutzi, M., et al. 2023b, PSJ, submitted

1554

1555   Chourey, S., Koschny, D., Rott, M., et al. 2020, P&SS, 194, 105112

1556

1557   Cueva, R. H., McMahon, J. W., & Meyer, A. J. 2023, PSJ, submitted

1558

1559 Daly, R. T., Ernst, C. M., Barnouin, O. S., et al. 2022, PSJ, 3(9), 207

1560

1561 Daly, R. T., Ernst, C. M., Barnouin, O. S. et al. 2023a, Nature, 616, 443-447

1562

1563 Daly, T. R., Ernst, C. M., Barnouin, O. S. et al. 2023b, PSJ, submitted

1564

1565 de León, J., Licandro, J., Duffard, R., & Serra-Ricart, M. 2006, AdSpR, 37,
1566 178-183

1567

1568 DeCoster, M. E., Luther, R., Collins, G. S., et al. 2023a, PSJ, submitted

1569

1570 DeCoster, M. E., Stickle, A. M., Rainey, E. S. G., & Graninger, D. 2023b,
1571 PSJ, submitted

1572

1573 Deshapriya, J. D. P., Hasselmann, P. H., Gai, I., et al. 2023, PSJ, in press

1574

1575 Dotto, E., Della Corte, V., Amoroso, M., et al. 2021, P&SS, 199, 105185

1576

1577 Dotto, E. & Zinzi, A. 2023, NatCo, 14, 3055

1578

1579 Dotto, E., Deshapriya, J. D. P., Gai, I. et al. 2023, Nature, submitted

1580

1581 Dunn, T. L., Burbine, T. H., Bottle, W. F., & Clark, J. P. 2013, Icar, 222,
1582 273-282

1583

1584 Durda, D. D., Walker, J. D., Chocron, S., et al. 2019, P&SS, 178, 104694

1585

1586 Ericksen, P. S., Chen, M., Haque M., et al. 2023, in GNC Conf, AAS 23-154

1587

1588 Ernst, C. M., Barnouin, O. S., Daly, R. T., et al. 2018, in LPSC 49, 1043

1589

1590 Ernst, C. M., Daly, R. T., Fletcher, Z. J., et al. 2023, PSJ, submitted

1591

1592 Fahnestock, E. G., Cheng, A. F., Ivanovski, S., et al. 2022, PSJ, 3(9), 206

1593

1594 Farnham, T. L., Hirabayashi, M., Deshapriya, J. D. P., et al. 2023, in ACM
1595 Conf, 2127

1596

1597 Ferrari, F., Raducan, S. D., Soldini, S., & Jutzi, M. 2022, PSJ, 3(7), 177

1598

1599 Ferrari, F., Panicucci, P., Merisio, G., et al. 2023, NatAs, submitted

1600

1601 Fitzsimmons, A., Berthier, J., Denneau, L., et al. 2023, in ACM Conf, 2452

1602

1603 Fletcher, Z. J., Ryan, K. J., Maas, B. J., et al. 2018, in 2018SPIE, 106981X

1604

1605 Fletcher, Z. J., Ryan, K. J., Ernst, C. M., et al. 2022, in 2022SPIE, 121800E

1606

1607 Flynn, G. J., Durda, D. D., Patmore, E. B., et al. 2015, P&SS, 107, 64-76

1608

1609 Flynn, G. J., Durda, D. D., Molesky, M. J., et al. 2020, IJIE, 136, 103437

1610

1611 Graninger, D., Stickle, A., Owen, J. M., & Syal, M. 2023, IJIE, 180, 104670

1612

1613 Gray, Z., Bagnulo, S., Granvik, M., et al. 2023, PSJ, submitted

1614

1615 Graykowski, A., Lambert, R. A., Marchis, F., et al. 2023, Nature, 616, 461-
1616 464

1617

1618 Hasselmann, P. H., Della Corte, V., Pravec, P., et al. 2023, PSJ, submitted

1619

1620 Heistand, C., Thomas, J., Tzeng, N., et al. 2019, in 2019 IEEE Aerospace
1621 Conference, 1-16

1622

1623 Hirabayashi, M., Davis, A. B., Fahnestock, E. G., et al. 2019, AdSpR, 63(8),
1624 2515-2534

1625

1626 Hirabayashi, M., Ferrari, F., Jutzi, M., et al. 2022, PSJ, 3(6), 140

1627

1628 Hirabayashi, M., Farnham, T. L., Deshapriya, J. D. P., et al. 2023, NatCo,
1629 submitted

1630

1631 Hoerth, T., Schäfer, F., Hupfer, J., Millon, O., & Wickert, M. 2015, Procedia
1632 Engineering, 103, 197-204

1633

1634 Holsapple, K. A. & Housen, K. R. 2012 Icar, 221, 875

1635

1636 Ieva, S., Mazzotta Epifani, E., Perna, D., et al. 2022, PSJ, 3(8), 183

1637

1638 Ieva, S., Mazzotta Epifani, E., Dotto, E., et al. 2023, PSJ, submitted

1639

1640 Ivanovski, S. L., Lucchetti, A., Zanotti, G., et al. 2023, PSJ, submitted

1641

1642 Jensenius, M. A., Chen, M., Ericksen, P., et al. 2023, in AIAA Guidance and
1643 Control Conference, AAS 23-135

1644

1645 Jewitt, D., Kim, Y., Li, J., & Mutchler, M. 2023, ApJ Lett, 952, L12

1646

1647 John, J., Roufberg, L., Ottman, G. K., and Adams, E. 2023, in 2023 IEEE
1648 Aerospace Conference, DOI: 10.1109/AERO55745.2023.10116014

1649

1650 Jutzi, M. & Michel, P. 2014, Icar, 229, 247-253

1651

1652 Kadono, T., Suetsugu, R., Arakawa, D., et al. 2019, ApJ Lett, 880, L30

1653

1654 Kareta, T., Thomas, C., Li, J.-Y., et al. 2023, ApJ Lett, in press

1655

1656 Kim, Y., & Jewitt, D. 2023, ApJ Lett, submitted

1657

1658 Kitazato, K. et al. 2004, LPSC XXXV, 1623

1659

1660 Kolokolova, L., Li, J., van Selous, M., Farnham, T. & Nagdimunov, L. 2022,
1661 PSJ, 3(11), 262

1662

1663 Kumamoto, K. M., Owen, J. M., Bruck Syal, M., et al. 2022, PSJ, 3(10), 237

1664

1665 Lazzarin, M., La Forgia, F., Migliorini, A., et al. 2023, PSJ, submitted

1666

1667 Li, J. -Y., Hirabayashi, M., Farnham, T. L., et al. 2023, Nature, 616, 452-
1668 456

1669

1670 Lin, Z.-Y., Vincent, J.-B. & Ip, W.-H. 2023, A&A, 676, A116

1671

1672   Lister, T., Constantinescu, C., Ryan, W., et al. 2023, PSJ, submitted
1673

1674   Liu, P.-Y., Campo Bagatin, A., Benavidez, P. G., & Richardson, D. C. 2023,
1675   Icar, submitted
1676

1677   Lolachi, R., Glenar, D. A., Stubbs, T. J. & Kolokolova, L. 2023, PSJ, 4, 24
1678

1679   Lucchetti, A., Cambioni, S., Nakano, R., et al. 2023, NatCo, submitted
1680

1681   Luther, R., Raducan, S. D., Burger, C., et al. 2022, PSJ 3(10), 227
1682

1683   Madeira, G., Charnoz, S., & Hyodo, R. 2023, Icar, 394, 115428
1684

1685   Makadia, R., Raducan, S. D., Fahnestock, E. G. & Eggl, S. 2022, PSJ, 3(8),
1686   184
1687

1688   Makadia, R., Chesley, S. R., Farnocchia, D., et al. 2023, PSJ, submitted
1689

1690   Meyer, A. J., Gkolias, I., Gaitanas, M., et al. 2021, PSJ 2(6), 242
1691

1692   Meyer, A. J., Scheeres, D. J., Agrusa, H. F., et al. 2023a, Icar, 391, 115323
1693

1694   Meyer, A. J., Agrusa, H. F., Richardson, D. C., et al. 2023b, PSJ, 4, 141
1695

1696   Michel, P., Cheng, A., Küppers, M., et al. 2016, ASpR, 57(12), 2529-2547
1697

1698   Michel, P., Kueppers, M., Sierks, H., et al. 2018, ASpR, 62, 2261-2272
1699

1700   Michel, P., Küppers, M., Campo Bagatin, A., et al. 2022, PSJ, 3(7), 160
1701

1702   Milani, A., Valsecchi, G., Paolicchi, P., et al. 2004,
1703   ESA https://doi.org/10.5270/don-quijote-exec-summ-2003
1704

1705   Miller, S. E., Pittelkau, M., Superfin, E., & O'Shaughnessy, D. 2023, in 12th
1706   ESA GNC and ICATT Conference
1707

1708   Moskovitz, N., Thomas, C., Pravec, P., et al. 2023, PSJ, in press
1709

1710 Moreno, F., Campo Bagatin, A., Tancredi, G., Liu, P., & Domínguez, B. 2022,
1711 MNRAS, 515(2), 2178-2187

1713 Moreno, F., Campo Bagatin, A., Tancredi, G., et al. 2023, PSJ, 4, 138

1715 Murphy, B. P., Opitom, C., Snodgrass, C., et al. 2023, PSJ, submitted

1717 Naidu, S. P., Margot, J. L., Taylor, P. A., et al. 2015, ApJ, 150:54

1719 Naidu, S. P., Benner, L. A. M., Brozovic, M., et al. 2020, Icar, 348, 113777

1721 Naidu, S. P., Chesley, S. R., Farnocchia, D., et al. 2022, PSJ, 3(10), 234

1723 Naidu, S. P., Chesley, S. R., Moskovitz, N., et al. 2023, PSJ, submitted

1725 Nakano, R., Hirabayashi, M., Agrusa, H. F., et al. 2022, PSJ, 3(7), 148

1727 Nakano, R., Hirabayashi, M., Raducan, S. D., et al. 2023, PSJ, submitted

1729 National Academies Press, 2010, Defending Planet Earth: Near-Earth Object
1730 Surveys and Hazard Mitigation Strategies; https://doi.org/10.17226/12842

1732 National Academies Press, 2022, Origins, Worlds, and Life: A Decadal Strategy
1733 for Planetary Science and Astrobiology 2023-2032, National Academies of
1734 Sciences, Engineering, and Medicine; https://doi.org/10.17226/26522

1736 Neese, C., Benner, L. A. M., and Ostro, S. J., Eds 2020, Asteroid Radar V1.0.
1737 urn:nasa:pds:compil.ast.radar-properties::1.0; NASA Planetary Data System;
1738 https://doi.org/10.26033/cqz1-et40.

1740 Opitom, C., Murphy, B., Snodgrass, C., et al. 2023, A&A, 671, L11

1742 Ormö, J., Raducan, S. D., Jutzi, M., et al. 2022, EPSL, 594, 117713

1744 Ostro, S. J., Margot, J.-L., Benner, L. A. M., et al. 2006, Science 314,
1745 5803, 1276-1280

1747 O'Shaughnessy, D. J. and Hefter, S. 2023, in GNC Conf, AAS 23-183

1748

1749 Owen, J. M., DeCoster, M. E., Graninger, D. M. & Raducan, S. D. 2022, PSJ,
1750 3(9), 218

1751

1752 Pajola, M., Barnouin, O. S., Lucchetti, A., et al. 2022, PSJ, 3(9), 210

1753

1754 Pajola, M., Tusberti, F., Lucchetti, A., et al. 2023, NatCo, submitted

1755

1756 Peña-Asensio, E., Küppers, M., Trigo-Rodríguez, J. M., & Rimola, A. 2023,
1757 PSJ, submitted

1758

1759 Penttilä, A., Muinonen, K., Granvik, M., at al. 2023, PSJ, submitted

1760

1761 Poggiali, G., Brucato, J. R., Hasselmann, P. H., et al. 2022, PSJ, 3(7), 161

1762

1763 Polishook, D., DeMeo, F. E., Burt, B. J. et al. 2023, PSJ, in press

1764

1765 Pravec, P., Benner, L. A. M., Nolan, M. C., et al. 2003, IAUC, 8244, 2

1766

1767 Pravec, P., Scheirich, P., Kušnirák, P., et al. 2006, Icar, 181, 63

1768

1769 Pravec, P., Harris, A. W., Kušnirák, P., Galád, A., & Hornoch, K. 2012, Icar,
1770 221, 365

1771

1772 Pravec, P., Scheirich, P., Kušnirák, P., et al. 2016, Icar, 267, 267

1773

1774 Pravec, P., Fatka, P., Vokrouhlick´y, D., et al. 2019, Icar, 333, 429

1775

1776 Pravec, P., Thomas, C. A., Rivkin, A. S. et al. 2022, PSJ, 3(7), 175

1777

1778 Pravec, P. Scheirich, P., Meyer, A. J., et al. 2023, ACM Conf, 2052

1779

1780 Raducan, S. D., Davison, T. M., Luther, R., & Collins, G.S. 2019, Icar, 329,
1781 282-295

1782

1783 Raducan, S. D, Davison, T. M. & Collins, G. S. 2020, P&SS, 180, 104756

1784

1785 Raducan, S. D., Jutzi, M., Davison, T. M., et al. 2021, IJIE, 162, 104147

1786

1787   Raducan, S. D. & Jutzi, M. 2022, PSJ, 3(6), 128

1788

1789   Raducan, S. D., Davison, T. M. & Collins, G. S. 2022a, Icar, 374, 114793

1790

1791   Raducan, S. D., Jutzi, M., Zhang, Y., Ormö, J., and Michel, P. 2022b, A&A,
1792   665, L10

1793

1794   Raducan, S. D., Jutzi, M., Cheng, A. F., et al. 2023a, NatAs, submitted

1795

1796   Raducan, S. D., Jutzi, M., Merrill, C. C., et al. 2023b, PSJ, submitted

1797

1798   Rainey, E. S. G., Stickle, A. M., Cheng, A. F., et al. 2020, IJIE, 142,
1799   103528

1800

1801   Richardson, D. C., Agrusa, H. F., Barbee, B., et al. 2022, PSJ, 3(7), 157

1802

1803   Richardson, D. C., Agrusa, H. F., Barbee, B. et al. 2023, PSJ, submitted

1804

1805   Rivkin, A. S. & Cheng, A. F. 2023 NatCo, 14, 1003

1806

1807   Rivkin, A. S., Chabot, N. L., Stickle, A. M., et al. 2021, PSJ, 2(5), 173

1808

1809   Rivkin, A. S., Thomas, C. A., Wong, I., et al. 2023, PSJ, in press

1810

1811   Robin, C. Q., Murdoch, N., Duchene, A., et al. 2023, NatCo, submitted

1812

1813   Rossi, A., Marzari, F., Brucato, J. R., et al. 2022, PSJ, 3(5), 118

1814

1815   Roth, N. X., Milam, S. N., Remijan, A. J., et al. 2023, PSJ, 4, 206

1816

1817   Rożek, A., Snodgrass, C., Jørgensen, U. G., et al. 2023, PSJ, in press

1818

1819   Rozitis, B., Green, S. F., Jackson, S. L., et al. 2023, PSJ, submitted

1820

1821   Rush, B. P., Mages, D. M., Vaughan, A. T., Bellerose, J., & Bhaskaran, S.
1822   2023, 33rd AAS/AIAA Space Flight Mechanics Meeting, AAS 23-234, 1-20

1823

1824 Sawyer, C. A., Fletcher, Z., Cheng, A. F., et al. 2023 in GNC Conf, AAS 23-
1825 111
1826
1827 Scheirich, P., & Pravec, P. 2009, Icar, 200, 531
1828
1829 Scheirich, P. & Pravec, P. 2022, PSJ, 3(7), 163
1830
1831 Scheirich, P. Pravec, P., Meyer, A. J., et al. 2023, PSJ, submitted
1832
1833 Shapiro, B. N. and Rodovskiy, L. 2023, 45th Rocky Mountain AAS GN&C
1834 Conference, AAS 23-181
1835
1836 Shestakova, L. I., Serebryanskiy, A. V., Krugov, M. A., Aimanova, G. K., &
1837 Omarov. Ch. T. 2023, RNAAS, 6, 223
1838
1839 Smith, E., Zhan, S., Adams, E., et al. 2020, IEEE Aerospace Conference, 1-9
1840
1841 Statler, T. S., Raducan, S. D., Barnouin, O. S., et al. 2022, PSJ, 244
1842
1843 Stickle, A. M., Atchison, J. A., Barnouin, O. S., et al. 2015, Procedia
1844 Engineering, 103, 577-584
1845
1846 Stickle, A. M., Rainey, E. S. G., Bruck Syal, M., et al. 2017, Procedia
1847 Engineering, 204, 116-123
1848
1849 Stickle, A. M., Bruck Syal, M., Cheng, A. F., et al. 2020, Icar, 338, 113446
1850
1851 Stickle, A. M., DeCoster, M. E., Burger, C., et al. 2022, PSJ, 3(11), 248
1852
1853 Stickle, A. M., Kumamoto, K. M., DeCoster, M. E., et al. 2023, NatCo,
1854 submitted
1855
1856 Superfin, E. A., O'Shaughnessy, D., Mages, D., et al. 2023, in AAS Guidance,
1857 Navigation, and Control Conference, AAS 23-096
1858
1859 Tancredi, G., Liu, P-Y, Campo-Bagatin, A., Moreno, F., & Domínguez, B. 2022,
1860 MNRAS, 522(2), 2403-2414
1861

1862 Thomas, C. A., Naidu, S. P., Scheirich, P., et al. 2023a, Nature, 616, 448-
1863 451
1864
1865 Thomas, C. A., Rivkin, A. S., Wong, I., et al. 2023b, ACM Conf, 2588
1866
1867 Tropf, B. T., Haque, M., Behrooz, N., & Krupiarz, C. 2023, IEEE SMC-IT,
1868 doi:10.1109/SMC-IT56444.2023.00020
1869
1870 Vincent, J.-B., Asphaug, E., Varnouin, O., et al. 2023, NatCo, submitted
1871
1872 Walker, J. D., Chocron, S., Durda, D. D., et al. 2013, IJIE, 56, 12-18
1873
1874 Walker, J. D., Chocron, S., Grosch, D. J., Marchi, S., & Alexander A. M.
1875 2022, PSJ, 3(9), 215
1876
1877 Waller, C. D., Espititu, R. C., Tinsman, C., et al. 2023, PSJ, submitted
1878
1879 Walsh, K. J. & Jacobson, S. A. 2015, in Asteroids IV, 375-393
1880
1881 Watanabe, S., Hirabayashi, M., Hirata, N., et al. 2019, Science, 364, 6437,
1882 268-272
1883
1884 Weaver, H. A., Sunshine, J. M., Ernst, C. M., et al. 2023, PSJ, submitted
1885
1886 Wolters, S. D., Ball, A. J., Wells, N., Saunders, C., & McBride, N. 2011,
1887 P&SS, 59, 1506
1888
1889 Zhan, S., Bekker, D., Boye, J., et al. 2021, IEEE Aerospace Conference
1890 (50100), 1-11
1891
1892 Zinzi, A., Della Corte, V., Barnouin, O. S., et al. 2023, LPSC,2021